Human CD4/CD8 double positive T cells are both predictive and sufficient to mediate GVHD pathology

Nicholas J. Hess[1,2], David Turicek[1], Jeremiah Riendeau[3,4], Sean McIlwain[5], Emmanuel Contreras Guzman[3,4], Kalyan Nadiminti[2,8], Amy Hudson[6], Natalie Callander[2], Melissa C. Skala[3,4], Jenny E. Gumperz[7,8], Peiman Hematti[2,8], *Christian M. Capitini[1,8]

[1]Department of Pediatrics, University of Wisconsin School of Medicine and Public Health, Madison, WI

[2]Division of Hematology/Oncology, Department of Medicine, University of Wisconsin School of Medicine and Public Health, Madison, WI

[3]Morgridge Institute for Research, Madison, WI

[4]Department of Biomedical Engineering, University of Wisconsin-Madison, Madison, WI

[5]Department of Biostatistics and Medical Informatics, University of Wisconsin-Madison, Madison, WI

[6]Department of Microbiology and Immunology, Medical College of Wisconsin, Milwaukee, WI

[7]Department of Medical Microbiology and Immunology, University of Wisconsin School of Medicine and Public Health, Madison, WI

[8]University of Wisconsin Carbone Cancer Center, Madison, WI

21 ***Corresponding Author**:

22 Christian M. Capitini

23 University of Wisconsin School of Medicine and Public Health

24 WIMR 4137, 1111 Highland Ave

25 Madison, WI 53705

26 Office: (608) 262-2415

27 Fax: (608) 265-9721

28 Email: ccapitini@pediatrics.wisc.edu

29 ORCID: 0000-0001-5720-9305 (NJH); 0000-0003-1852-2192 (JG)

30

31 **Abstract Word Count = 197**

32 **Word Count = 9572**

33 **Reference Count = 58**

34

35 **Running Title: DPTs Are Predictive and Sufficient for GVHD**

Abstract

An important paradigm to improve allogeneic hematopoietic stem cell transplantations (allo-HSCTs) is the prevention of graft-vs-host disease (GVHD) while preserving the beneficial graft-vs-leukemia (GVL) activity of donor T cells. In an observational clinical study of adult allo-HSCT recipients, we identified five T cell specific predictive biomarkers of relapse and GVHD. One interesting biomarker was the emergence of a CD4/CD8 double positive T cell (DPT) population not present in the starting graft tissue. Using a xenogeneic transplant model to investigate this population further, we also reveal that DPTs are predictive of lethal GVHD irrespective of donor or graft source. We observed that DPTs originated from the CD8 T cell population, co-expressed both RUNX3 and THPOK and are not the by-product of a lymphodeplete environment. Further transcriptomic, metabolomic and functional assays all revealed DPTs to be a highly activated T cell population distinct from both CD4 and CD8 T cells. Importantly, DPTs isolated from GVHD mice were sufficient to mediate xenogeneic GVHD after re-transplantation but had no observable GVL activity when challenged in vivo with two human B-ALL malignancies. Overall, these studies highlight a GVHD-specific human T cell population with the potential to delineate GVL activity from GVHD pathology.

52 **Introduction**

53 Graft-vs-host disease (GVHD) and relapse remain the primary complications following an
54 allogeneic hematopoietic stem cell transplantation (allo-HSCT)[1–3]. While the field has made
55 significant strides in reducing GVHD in the recent decade, current GVHD prophylaxis drug
56 regimens target the entire T cell population, potentially hindering the efficacy of graft-vs-leukemia
57 (GVL) activity mediated by donor T cells[4–8]. Thus, identifying predictive biomarkers and
58 delineating specific cellular mechanism(s) leading to GVHD pathology versus GVL activity has
59 remained a top priority for the field.

60

61 Unfortunately, separating the graft-vs-host (GVH) response of donor T cells from their GVL activity
62 has proven difficult as both responses are derived from allogeneic antigen stimulation[7–9].
63 Nevertheless, several studies have investigated the role of specific HLA mismatches on the
64 development of GVHD and GVL activity[10–13]. These studies have highlighted the importance of
65 permissive and non-permissive HLA mismatches on GVHD development and non-relapse
66 mortality but correlating them with GVL activity has been met with limited success[10–14].
67 Furthermore, the use of haploidentical transplantations with post-transplant cyclophosphamide
68 has shown that HLA matching of the donor and recipient may not play a dominant role in
69 separating GVH and GVL activity[15,16].

70

71 While pre-transplant prognostic variables such as HLA-matching, conditioning regimens and graft
72 source all influence allo-HSCT outcomes, these population-based variables are not able to predict
73 individual patient outcomes[17–19]. Several post-transplant predictive variables have been
74 discovered including sST2, REG3α, elafin and others[20–26]. These highly promising plasma-based
75 biomarkers are generally released due to host damage and have shown efficacy in predicting the
76 development of steroid-resistant GVHD and non-relapse mortality (NRM) either individually or
77 combined into a predictive algorithm[20–26]. To date though, these biomarkers have not been able

78 to predict an allo-HSCT recipients' chance of relapse as they measure the degree of host damage
79 rather than donor T cell alloreactivity.
80
81 As the causative agent of both GVHD and GVL, the direct investigation of T cell populations has
82 been another area of active investigation[27–30]. Both CD4 and CD8 T cells can respond to
83 allogeneic antigens, but while CD8 T cell may be directly responsible for cellular cytotoxicity, CD4
84 T cells have recently been the primary focus of the field[31–33]. The CD4 population is unique in its
85 capacity to polarize into a variety of different subsets, based on the cytokine environment it finds
86 itself, to drive an inflammatory response[34–40]. In the case of GVHD, TH_1 and $TH_{17/22}$ cells have
87 been shown to be directly involved in driving the pathogenesis of gastrointestinal, liver and skin
88 pathology[35,41]. In contrast, the CD8 T cell population is thought to be fairly uniform in their role as
89 cytotoxic effectors licensed by CD4 T cells. The discovery of CD8 regulatory T cells in murine
90 GVHD though suggests CD8 T cells may also be able to polarize into different subsets similar to
91 the CD4 population[42,43]. Despite our increased understanding of GVHD pathogenesis mediated
92 allo-reactive T cells, T cell specific GVHD prophylaxis regimens have been slow to enter the clinic
93 and have not yet shown a direct cellular mechanism separating GVH from GVL activity.
94
95 Interestingly, several recent studies have now identified a novel human T cell population co-
96 expressing both CD4 and CD8 lineage markers in a variety of chronic inflammatory diseases,
97 including GVHD[44–51]. Historically, CD4/CD8 double positive T cells (DPTs) have only existed as
98 a developmental stage of T cells in the thymus that are unable to survive in the periphery due to
99 the lack of survival signals[52,53]. The presence of DPTs in the periphery of these human chronic
100 inflammatory diseases suggests either a breakdown in T cell development or that DPTs in the
101 periphery are a previously unidentified mature human T cell population with an unknown origin
102 and function[53].
103

104 In this study, we identify five T cell metrics capable of predicting relapse, GVHD or both in allo-
105 HSCT recipients several weeks to months prior to their diagnosis. One of these predictive
106 biomarkers was the frequency of DPTs which we explored further in a xenogeneic transplant
107 model. This xenogeneic transplant model was able to successfully recapitulate the development
108 and predictive potential of DPTs with lethal xenogeneic GVHD. We also reveal that DPTs alone
109 are sufficient to mediate GVHD pathology but have little GVL activity against two human B-ALL
110 cancer lines. This study also identifies the origin of DPTs as the CD8 T cell population. Overall,
111 this study describes the origin and function of a novel human T cell population that has clinical
112 significance in its ability to predict GVHD in allo-HSCT recipients and is sufficient for GVHD
113 pathology but not GVL activity in a xenogeneic transplant model.
114
115 **Results**
116
117 **T cell specific predictive biomarkers of relapse and GVHD in allo-HSCT recipients**
118 To determine if the direct measurement of T cells in allo-HSCT recipients post-transplant can
119 serve as predictive biomarkers of relapse and/or GVHD, we collected 417 blood samples from 35
120 adult allo-HSCT recipients over their first 100 days post-transplant (Fig 1A). Patients were
121 included in the observational study irrespective of their conditioning regimen, donor HLA
122 matching, graft source or GVHD prophylaxis regimen with the only requirement being they
123 received post-transplant cyclophosphamide (Supplemental Table 1). Samples were processed
124 within seven days of collection and never frozen. Antigen-experienced T cells were gated based
125 on CD3 and CD45RO expression as a means to exclude non-reactive donor T cells and naïve T
126 cells that are present due to de novo hematopoiesis (Supplemental Fig 1).
127
128 From a total of 11 T cell metrics analyzed, we identified five as having the capacity to predict
129 relapse, GVHD (of any grade) or ≥ grade 2 GVHD (Fig 1B). We first analyzed the samples

130 collected between days 7 and 17 in three binary tests to determine if any could significantly
131 differentiate between two allo-HSCT outcomes. Tests that were shown to be significant by t-test
132 were further evaluated using a receiver-operator-characteristic (ROC) analysis (Fig 1C). We
133 identified two predictive biomarkers of relapse (CD45RO T cells and frequency of Tregs), four
134 predictive biomarkers of GVHD (CD45RO T cells and the frequency of Tregs, CD8 and DPTs)
135 and two predictive biomarkers of ≥ grade 2 GVHD (frequency of Tregs and DPTs) (Fig 1C).
136 Combining the individual T cell metrics into one multi-parameter analysis further increased their
137 predictive potential as measured by the area-under-the-curve (AUC) values that reached 0.848,
138 0.736 and 0.701 for relapse, GVHD and ≥ grade 2 GVHD prediction respectively (Fig 1D).
139
140 A second analysis included patient samples collected between days 22 and 83 and were further
141 normalized relative to each individual patient's date of GVHD diagnosis (either grade 1 or 2). For
142 patients who did not develop GVHD, we normalized their data to day 54, which was the average
143 time to GVHD diagnosis among our cohort. In this analysis, only three of the original five T cell
144 biomarkers showed any predictive value with all three metrics predicting relapse (CD45RO T cells
145 and the frequencies of CD8 and DPTs) and the frequency of CD8 and DPTs predicting both GVHD
146 (of any grade) and ≥ grade 2 GVHD (Fig 1E). Combining the predictive metrics into one multi-
147 parameter analysis as before further increase their predictive value with AUC values of 0.892,
148 0.741 and 0.734 for relapse, GVHD and ≥ grade 2 GVHD prediction respectively (Fig 1F).
149
150 **Xenogeneic transplantation also reveals DPTs as a predictive biomarker of GVHD**
151 **development**
152 To replicate our clinical observational study, we utilized a human xenogeneic transplant model
153 wherein we transplanted various human graft tissue into immunodeficient mice[31,54,55]. As in our
154 observational clinical study, we observed the presence of DPTs, which were not present in the
155 starting healthy graft tissue, primarily developing in mice that would later develop lethal

156 xenogeneic GVHD (Fig 2A). We confirmed that DPTs are not an artifact of doublets by
157 ImageStream analysis, are not recent thymic emigrants by their lack of CD31 expression and
158 develop even when isolated human T cells are used for transplantation (Fig 2B, data not shown
159 and Supplemental Fig 2). DPTs were present in variety of GVHD target organs and developed as
160 early as 1wk after transplant in each of the four graft sources we tested (Fig 2C-H). The increased
161 frequency of DPTs was also a predictive biomarker of lethal GVHD development in this model
162 system at 1-, 3- and 6-weeks post-transplant (Fig 2I). We further confirmed that the frequency of
163 Tregs at 1-week after transplant could act as a predictive biomarker of lethal xenogeneic GVHD
164 but with the function of Tregs already well established, we chose to focus on the origin and
165 function of DPTs for the remainder of this study (Supplemental Fig 3).
166
167 **The DPT population is distinct from CD4 and CD8 T cells**
168 Two alternative hypotheses against DPT being a unique T cell population is the possibility that
169 CD4 T cells co-expressing CD8α upon activation or that CD4 or CD8 T cells could co-express the
170 alternative lineage marker through trogocytosis. To determine if either of these are possible, we
171 first show that DPTs express both CD8α and CD8β, suggesting this population is not the result of
172 an activated CD4 T cell population (Supplemental Fig 4A-B). Furthermore, we flow-sorted DPTs
173 from GVHD mice and expanded them in vitro and/or transplanted them into a naïve mouse. In
174 both cases, the DPT population persisted even in the absence of single positive CD4 and CD8 T
175 cells suggesting that co-expression of the CD4 and CD8 lineage markers is sustained and not the
176 result of trogocytosis (Supplemental Fig 4C-F). Additionally, the DPT population does not appear
177 to be the result of a dead/dying T cell population due to a high expression of the pro-survival
178 protein BCL2 (Supplemental Fig 4G).
179
180 To explore how T cells if the CD4 and CD8 lineage markers are actually co-transcribed, we
181 performed RNA-seq on flow-sorted CD4, CD8 and DPTs from GVHD mice (Fig 3). Analysis of the

182 transcriptome of these cells revealed that DPTs express a transcriptional signature unique from
183 CD4 or CD8 T cells (Fig 3A-B). Using a threshold of $p<0.01$ and a fold change of >10 to determine
184 significance, we reveal that DPTs differentially expressed 63 genes compared to CD4 and CD8
185 T cells (Fig 3A). Of the differentially expressed genes, we confirmed that both CD4 and CD8 are
186 both transcriptionally expressed in DPTs (Fig 3C-E). Interestingly, DPTs also appear to express
187 several genes normally associated with B cell biology though the mechanism for this observation
188 requires further investigation (Fig 3E).
189
190 Using all 796 genes differentially expressed in the DPT:CD4 and DPT:CD8 comparisons, KEGG
191 BRITE functional hierarchical classification highlighted numerous differentially expressed genes
192 serving as enzymatic genes along with CD molecules, exosome machinery, transcription factors
193 and cytokine/cytokine receptors (Supplemental Table 2). To explore possible expression
194 differences further, we surveyed 13 inflammatory and inhibitory co-receptors on the surface of
195 CD4, CD8 and DPTs from GVHD mice (Fig 4A-C, Supplemental Fig 5). Interestingly, DPT
196 displayed an intermediate expression of CD27, OX40, PD-1 and LAG3 compared to CD4 and
197 CD8 T cells analyzed from the blood or spleen of GVHD mice (Fig 4A-C, Supplemental Fig 5).
198 The expression of these markers was further explored on the T cells from our observational
199 clinical study (Fig 4D-L). While the expression of these markers differed slightly, most likely due
200 to differences in the mouse versus human host environment, DPTs still displayed an expression
201 profile of a terminally differentiated effector T cell population with little evidence of exhaustion (Fig
202 4D-L).
203
204 **DPTs differentiate from the CD8 T cell population and upregulate THPOK**
205 To identify the T cell population that gives rise to DPTs, we performed an unsupervised tSNE
206 clustering of human T cells from a xenogeneic GVHD mouse using a nine-color flow cytometry
207 panel (Fig 5A). This analysis, in addition to the global transcriptomic analysis, indicated that DPTs

208 cluster more closely with CD8 T cells than CD4 T cells. Thus, despite the well documented
209 plasticity of the CD4 lineage, our results suggest that DPTs may develop from the CD8 lineage
210 (Fig 3B, Fig 5A).
211
212 To test this hypothesis, we transplanted isolated CD4 or CD8 T cells from a healthy donor into
213 our xenogeneic transplant model. Elevated frequencies of DPTs were only observed in mice
214 transplanted with isolated CD8 T cells, indicating that mature CD8 T cells and not CD4 or
215 progenitor T cells give rise to the DPT population (Fig 5B-C). Clonal TCR analysis of the TRAB
216 gene within the CD4, CD8 and DPT populations also provide evidence that the CD4 and DPT
217 populations are experiencing clonal expansion. We identified fewer overall clones in the CD4 and
218 DPT populations when compared to the CD8 population. Furthermore, the top ten clones of both
219 the CD4 and DPT populations represent ~25% of the entire population while the top ten clones in
220 the CD8 population equal only half that number (Fig 3F, Supplemental Table 3).
221
222 To support our hypothesis that DPTs differentiate in response to xeno/allo-antigens and not as a
223 result of the lymphodeplete environment found with allo-HSCT recipients and NSG mice, we
224 surveyed the phosphorylation status of several STAT proteins. Downstream of a variety of
225 cytokine receptors, phosphorylated STAT proteins might offer insight into the development of
226 DPTs. Unfortunately, we could not identify any differences in the phosphorylation of STAT1, 3, 4
227 and 6 between the CD8 and DPT populations (Supplemental Fig 6A-B). Furthermore, the
228 transplantation of CD4 or CD8 T cells sorted from a previously transplanted xenogeneic GVHD
229 mouse into a naïve mouse did not result in any DPTs emerging (Fig 5D-F). This suggests to us
230 that the emergence of DPTs is not the result of the lymphodeplete or xenogeneic environment
231 and is instead, the result of unknown activation events that occur early post-transplant in the CD8
232 T cell population.
233

234 Knowing that the transcriptome of DPT is unique compared to CD8 T cells and that transcription
235 factors was one of the functional analyses highlighted in the KEGG BRITE analysis, we further
236 investigated what transcription factors may be involved in the differentiation of DPT from the CD8
237 population. Interestingly, we observed that the transcriptional expression of the CD4 lineage
238 master transcription factor, THPOK (ZBTB7B) was upregulated compared to CD8 T cells (Fig 5G-
239 H). DPTs also displayed elevated levels of the CD8 lineage master transcription factor, RUNX3,
240 relative to CD4 T cells (Fig 5G-H). This dual expression of both CD4 and CD8 lineage master
241 transcription factors was confirmed by flow cytometry which showed DPTs expressing an
242 intermediate amount of each transcription factor relative to their single positive T cell controls (Fig
243 5I-J). DPT also displayed differences in the polarizing transcription factor T-bet (TBX21) which
244 was increased relative to CD4 T cells but decreased relative to CD8 T cells (Supplemental Fig
245 6C-E). There was also a small increase in the expression of RORγt relative to CD8 T cells, a
246 decrease in FOXP3 expression relative to CD4 T cells and no difference in GATA3 expression
247 (Supplemental Fig 6C-E).
248
249 **Differentiated DPTs are a metabolically active and unique T cell population**
250 To further explore DPT biology, we investigated their metabolic state relative to CD4 and CD8 T
251 cells. We analyzed sorted CD4, CD8 and DPTs from xenogeneic mice using a two-photon (2P)
252 autofluorescence imaging system (Fig 6A-E). This system is able to detect the autofluorescence
253 of NAD(P)H and FAD at a single cell resolution and use their ratios to determine the optical redox
254 ratio (ORR) of the cell population as a measurement of metabolic activity[56,57]. This analysis
255 revealed that the DPT population had elevated ORR, indicative of high metabolic activity (Fig 6A-
256 B). Furthermore, a random forest classifier trained to integrate the 10 metabolic parameters
257 imaged accurately identified the DPT population from CD4 and CD8 T cells (Fig 6C-E). This is
258 shown as a confusion matrix, ROC curve and a UMAP dimensionality reduction (Fig 6C-E).
259 Additional metabolic analysis using a Seahorse real-time metabolic analyzer independently

260 confirmed that DPTs have a higher ATP production rate than CD4 and CD8 T cells with the
261 increased ATP production primarily coming from glycolysis (Fig 6F). In addition to metabolic
262 differences, we also analyzed the T cell populations for evidence of “blasting”. Blasting is
263 characterized by increased cell size and is marker of cellular proliferation in T cells. The DPT
264 population displayed higher frequencies of the blasting phenotype relative to CD8 T cells in both
265 xenogeneic and clinical GVHD samples (Supplemental Fig 7).
266
267 **DPTs represent a GVHD-specific T cell population with little GVL activity**
268 To confirm the role of DPTs in the pathology of xenogeneic GVHD, we flow-sorted CD4, CD8 and
269 DPTs from GVHD mice and re-transplanted each population individually into naïve mice (Fig 7A).
270 Interestingly, only DPTs caused lethal xenogeneic GVHD (Fig 7B-C). DPTs expanded rapidly
271 after transplantation and had increased infiltration into the spleen, liver, and lungs relative to CD4
272 and CD8 T cells (Fig 7D-F). Mice transplanted with DPTs also exhibited high levels of human
273 IFNγ in their plasma compared to CD8 T cells (Fig 7G). To further investigate the cytokine
274 repertoire of DPTs, we cultured human T cells from GVHD mice overnight with brefeldin A prior
275 to intracellular cytokine staining. DPTs secreted a diverse repertoire of cytokines including the
276 cytotoxic granzyme and perforin, the inflammatory modulators IL-17A, IL-22 and GM-CSF as well
277 as the general activation cytokines IFNγ and TNFα (Fig 6H-I, Supplemental Fig 8). These data
278 highlight the extreme pro-inflammatory state of DPTs and reveal this population to be the primary
279 mediator of xenogeneic GVHD pathology.
280
281 While we have shown evidence that DPTs are sufficient to mediate GVHD pathology, we next
282 wanted to determine if they can also mediate GVL activity against two human B-ALL
283 malignancies. Human B-ALL cell lines were injected seven days prior to the transplantation of
284 CD4, CD8 or DPTs flow-sorted from GVHD mice (Fig 8A). Relative to control mice only receiving
285 the B-ALL cell line NALM-6, both flow-sorted CD4 and CD8 T cells were able to prolong survival

286 while DPTs provided no survival advantage (Fig 8B). The extended survival of mice given flow-
287 sorted CD4 and CD8 T cells was due to their ability to control the expansion of NALM-6 as seen
288 by IVIS and flow cytometry quantification of the number of NALM-6 cells in the blood of these
289 mice. The failure of DPTs to prolong survival was not due to a lack of cells within the mouse or a
290 failure of activation as measured by IFNγ (Fig 8E-F). In fact, sorted CD8 T cells were able to
291 prolong survival even in the absence of detectable IFNγ suggesting they maintain some GVL
292 activity even without CD4 T cell help (Fig 8F). An in vitro cytotoxicity assay of the flow-sorted T
293 cell populations also revealed that DPTs had a three-fold lower capacity to kill NALM-6 compared
294 to flow-sorted CD4 and CD8 T cells (Fig 8G). Next, we determined if there were any differences
295 between flow sorted CD4 and CD8 T cells from a GVHD mouse and freshly isolated CD4 and
296 CD8 T cells from a healthy donor. We reveal that fresh CD4 and CD8 T cells provided a similar
297 survival advantage as before, highlighting that flow sorted CD4 and CD8 T cells from GVHD mice
298 do not lose their capacity to mediate GVL activity (Supplemental Fig 9). To ensure this result is
299 not specific to NALM-6, we tested flow-sorted CD4, CD8 and DPTs against a second B-ALL cell
300 line, RS4;11. DPTs also failed to protect against RS4;11 while flow-sorted CD4 and CD8 T cells
301 were able to prolong survival (Fig 8H-K). These results suggest that the DPT population, which
302 differentiates from the CD8 T cell population after transplant, may represent a GVHD-specific T
303 cell population with limited GVL activity against human B-ALL malignancies.
304

305 **Discussion**

306 In this study, we identified five novel T cell specific predictive biomarkers of relapse and GVHD
307 which included a unique CD4/CD8 double positive T cell (DPT) population. Human DPTs originate
308 from the CD8 population after transplant through a currently unknown mechanism and are
309 transcriptionally, metabolically, and functionally distinct from CD4 and CD8 T cells. Furthermore,
310 we revealed that DPTs are sufficient for GVHD pathology when transplanted into naïve NSG mice
311 but possess little GVL activity against two human B-ALL cell lines. With DPTs also being identified

312 in other human chronic inflammatory diseases beyond GVHD, the molecular characterization of
313 DPTs in this manuscript may provide additional insight into the pathogenesis of these complex
314 diseases.
315
316 The identification of novel predictive biomarkers of allo-HSCT outcome is an important endeavor
317 that many groups have investigated in the past using serum analytes as biomarkers[17–19]. As such,
318 the direct investigation of T cells as a source of predictive biomarkers represents an exciting new
319 field of biomarker research. Our results here support the hypothesis that T cell metrics can predict
320 allo-HSCT outcomes early after transplant and independent of most pre-transplant prognostic
321 variables currently used in the clinic (Supplemental Table 1). While the use of T cell predictive
322 biomarkers still have to be validated in a larger multi-center study, this study highlights their
323 potential as a biomarker capable of predicting both relapse and GVHD after transplant.
324
325 To identify the five T cell predictive biomarkers in this study, we gated solely on the CD45RO$^+$ T
326 cell population. The gating on CD45RO$^+$ T cells is based on the knowledge that CD45RO is only
327 expressed on effector and memory T cells and the hypothesis that gating on this effector/memory
328 T cell population would provide additional sensitivity and reduce the “noise” in the system. With a
329 patient’s conditioning regimen eliminating or reducing their own T cell numbers to very low levels,
330 we hypothesize that the CD45RO$^+$ T cell population we are measuring is predominantly donor T
331 cells. Thus, we are using CD45RO as a marker to identify donor effector T cells that are activated
332 against either host or leukemia antigen. While we acknowledge that this gating strategy is not
333 specific for effector T cells, it allows us to remove naïve, non-reactive T cells coming from the
334 donor graft and naïve T cells generated de novo from hematopoiesis which increases the
335 sensitivity of our T cell biomarkers.
336
337 Of the five T cell predictive biomarkers we identified, only DPTs lacked a verified biological

338 function. One recent manuscript which also identified DPTs in GVHD patients suggested that they
339 possess a regulatory function[44]. In our own analysis, we observed that an increase in the
340 percentage of DPTs was predictive of GVHD suggesting a positive correlation with pathology. In
341 our functional characterization of DPTs, we identified them as a highly activated T cell population
342 that expressed pro-inflammatory cytokines including IFNγ, TNFα, IL-17A, IL-22 and GM-CSF in
343 addition to the cytotoxic cytokine's perforin and granzyme (Fig 6H-I, Supplemental Fig 7).
344 Furthermore, DPTs did not display classical markers of exhaustion in our xenogeneic transplant
345 model, with their expression of PD-1, LAG3, TIGIT, TIM3 and CTLA4 all at or below CD4 or CD8
346 single-positive controls (Fig 4B-C, Supplemental Fig 5). This observation is further supported in
347 our clinical observation study where we show that DPTs express low levels of PD-1, TIGIT and
348 lack the expression of LAG3 (Fig 4D-L). Our additional metabolic studies revealed they exist in
349 an activated state that, when re-transplanted in naïve mice, are sufficient to mediate GVHD
350 pathology (Fig 7). These data support our conclusion that DPTs represent a highly inflammatory
351 T cell population that are directed involved in pathology.
352
353 In addition to showing that DPTs are sufficient for lethal GVHD pathology, we also provide
354 evidence that they have limited GVL activity (Fig 7-8, Supplemental Fig 8). This surprising
355 observation is offset slightly by our inability to deplete DPTs without also depleting CD4 and/or
356 CD8 single-positive T cells. Currently, we have not identified a DPT specific marker uniquely
357 expressed by this population, which would have allowed us to confirm the DPT population is not
358 required for GVL activity. Without this tool, we are unable to conclude that DPTs do not possess
359 any GVL activity but our experiments with flow sorted CD8 T cells from GVHD mice do support
360 that conclusion. Flow-sorted CD8 T cells transplanted into naïve mice did not cause any signs of
361 GVHD but were still able to delay the B-ALL induced death of mice without signs of any new DPT
362 population forming (Fig 7 & 8). While not conclusive, these data highlight the exciting possibility
363 that a DPT-specific immunotherapy may one day allow for the prevention of GVHD without

364 inhibiting GVL activity.

365

366 With the CD4 T cell lineage have a well-established plasticity for different polarization states, we
367 were surprised to identify CD8 T cell as the origin of DPTs (Fig 5)[34,37–39]. Other than a CD8/FOXP3
368 regulatory T cell population, there are few other polarization states of CD8 T cells that have been
369 identified[42,43]. Furthermore, the master transcription factors of the CD8 and CD4 lineages, RUNX3
370 and THPOK respectively, are thought to negatively regulate each other[52]. While RUNX3 and
371 THPOK are both expressed in thymocytes during T cell development, mature T cells are thought
372 to be lineage restricted due to this process[52]. It was thus surprising that DPTs expressed both
373 RUNX3 and THPOK, both at the level of transcription and protein, via a currently unknown
374 mechanism. As such, additional studies will be required in the future to understand the signaling
375 and epigenetic mechanism(s) associated with this dual transcription factor expression (Fig 5).

376

377 Overall, this study uncovers the previously unknown origin and function of a human CD4/CD8
378 DPT population that is also a predictive biomarker of GVHD in adult allo-HSCT patient samples.
379 Metabolic, transcriptomic, and functional studies all identified DPTs as a T cell population with
380 distinct properties from single-positive CD4 and CD8 T cells. This highly inflammatory state
381 resulted in lethal GVHD pathology when isolated DPTs were transplanted into naïve NSG mice
382 while CD4 and CD8 T cells populations, also isolated from GVHD mice, failed to cause lethal
383 pathology after re-transplantation. The DPT population though could not control two human B-
384 ALL cell lines, suggesting that the development of this population from the CD8 T cell population
385 might be dependent on chronic antigen stimulation from the host. Future studies will need to
386 explore the connection of DPTs with other human chronic inflammatory disorders they have been
387 identified in including rheumatoid arthritis, hepatitis B and C, β-thalassemia, renal carcinomas,
388 breast cancers and islet graft rejection[45–51]. In conclusion, DPTs represent a unique T cell
389 population whose presence should be directly investigated in other human chronic inflammatory

390 diseases.

391

392 **Methods**

393 *Isolation of Primary Human Cells.* Human peripheral blood was collected from healthy consenting
394 donors according to IRB protocol 2014-0806 (J.E.G.) and 2017-1070 (C.M.C). Leftover and de-
395 identified remnants of human bone marrow and G-CSF mobilized peripheral blood grafts used for
396 allo-HSCT procedures at our clinic were collected under IRB protocol 2016-0298 (P.H.). De-
397 identified human umbilical cord blood was collected from the Medical College of Wisconsin's cord
398 blood bank. All human blood samples were diluted 1:1 with leukocyte isolation buffer (PBS, 2mM
399 EDTA, 2% FBS) prior to ficoll density-gradient centrifugation (1100xg for 15 min with 0 brake).
400 When indicated, StemCell Technologies RosetteSep T cell, CD4 or CD8 enrichment kits were
401 used.

402

403 *Clinical Sample Collection.* All patients receiving an allo-HSCT at the University of Wisconsin-
404 Madison were prospectively enrolled between October 2020 and August 2021 on the minimal-
405 risk IRB protocol 2020-1490 (C.M.C.). A total of 35 patients were enrolled on this study. Eligible
406 patients had to receive post-transplant cyclophosphamide for GVHD prophylaxis at day +3/+4.
407 Conditioning regimen, HLA matching status, graft source and patient disease type were all non-
408 exclusion criteria for this study. Patients were divided into four respective categories based on
409 their allo-HSCT outcome: no GVHD, grade 1 GVHD, grade 2 GVHD or grade 3-4 GVHD. Patient
410 assignment into each respective GVHD category is based on their highest GVHD grade achieved
411 between day 0 and 100 after transplant. The development of GVHD after day 100 was not factored
412 into this analysis.

413

414 Excess blood from study patients was set aside after initial use and stored at 4ºC for 3-10 days
415 before processing and was never frozen. A total of 0.5mL of blood was aliquoted from each patient

416 collection tube for each flow cytometry test and centrifuged at 600xg for 4min at 4ºC. The cell
417 pellet was resuspended in 1.5mL of 1X RBC lysis buffer (BioLegend), vortexed and rested for
418 2min prior to washing with 1mL of PBS and centrifugation. Supernatant was disposed of and a
419 second round of RBC lysis was performed. Afterwards, the cell pellet was re-suspended in 1.5mL
420 of flow buffer (1X PBS + 2% FBS) and aliquoted into three flow cytometry tubes for staining.
421
422 *Transplantation of human cells into NSG Mice*. All human cells were washed and resuspended in
423 150µL/mouse of sterile 1X PBS prior to retro-orbital injection. Equal numbers of male and female
424 immunodeficient NSG (NOD.Cg-*Prkdc*^{scid} *Il2rg*^{tm1Wjl}/SzJ) between the ages of 8-16 weeks of age
425 were used for all experiments. All mice were weighted and monitored weekly for visible signs of
426 GVHD with a scoring system carried out as follows: 0 = no signs of GVHD; 1 = 2-5% weight loss;
427 2 = 6-9% weight loss; 3 = 10-14% weight loss; 4 = ≥ 15% weight loss. Blood was regularly drawn
428 at 1, 3, 6, 9- and 12-weeks post-transplant by retro-orbital bleeding. At time of euthanasia, the
429 spleen, one lobe of the liver, lungs and femur were regularly collected for further processing.
430
431 *Flow Cytometry and Cell-Sorting.* All cells were stained in flow buffer (PBS, 10% FBS) prior to
432 quantification on a ThermoFisher Attune NxT Flow Cytometer and analysis on FlowJo V10.
433 Antibody clones include mCD45 (A20), ICOS (C398.4A), T-bet (4B10), LAG3 (11C3C65), FASL
434 (NOK-1), CD4 (OKT4), CD69 (FN50), OX40 (Ber-ACT35), CD27 (O323), pSTAT4 (p38), RORγt
435 (Q21-559), CD44 (BJ18), NKG2D (1D11), PD-1 (EH12.2H7), THPOK (ZFP-67), TIGIT
436 (A15153G), CD45RO (UCHL1), TIM3 (F38-2E2), pSTAT6 (A15137E), IL-22 (2G12A41), GATA3
437 (16E10A23), CD8α (RPA-T8), CD8β (SIDI8BEE), CD25 (BC96), 4-1BB (4B4-1), CD28 (CD28.2),
438 RUNX3 (SD0803), CTLA4 (BNI3), PanHLA (w6/32), CD3 (UCHT1). Visualization of cells was
439 complete using an ImageStream Mark II.
440

441 For cell sorting, cells were collected from the blood, spleen, liver and lungs of mice transplanted
442 with a lethal dose of PB-MNC approximately 4 weeks prior. Processed tissues were ficolled as
443 described above to obtain mononuclear cells. Human cells were isolated from the combined
444 mononuclear cells using StemCell Technologies EasySep Mouse/Human Chimera isolation kit.
445 Human cells were then stained in sterile PBS with the human CD4 (OKT4) and CD8β (SIDI8BEE)
446 antibodies prior to sorting on a BD FACSAria Cell Sorter. Cells were then maintained in cell culture
447 for 2-3 days prior to transplantation and/or expansion.
448
449 *Cell Lines and Cell Culture.* The human B-ALL line RS4;11 and NALM-6 were purchased from
450 ATCC and cultured using standard RPMI-10 media (RPMI base media, 10% FBS, 1X Pen/Strep,
451 1mM NEAA, 1X GlutaMAX). After flow sorting, isolated human CD4, CD8 and DPT populations
452 were expanded by co-culturing with a 10X dose of γ-irradiated (25Gy) human mononuclear cells
453 from a third-party donor with 5μg/mL of PHA in RPMI-10 media supplemented with 5ng/mL of
454 human IL-2 and IL-7. RPMI-10 media supplemented with IL-2 and IL-7 was added/changed
455 approximately every 3-4 days.
456
457 *mRNA sequencing.* T cells from five GVHD mice were pooled prior to flow-sorting of the CD4,
458 CD8 and DPTs. Pooled T cell populations were then split into three replicates for RNA isolation.
459 All RNA isolation and sequencing was performed by the Gene Expression Center at the University
460 of Wisconsin-Madison. RNA was isolated with Qiagen RNeasy kit prior to a quality control check
461 using an Agilent Bioanalyzer and NanoDrop One spectrophotometer. mRNA libraries were
462 prepared using the TruSeq stranded mRNA kit and sequenced on an Illumina NovaSeq 6000
463 platform to 30 million reads per sample. Sample reads were processed by the University of
464 Wisconsin Biotechnology Center.
465

466 *ELISAs.* Mouse blood samples were diluted with 50μL of 1X PBS prior to centrifugation with 60μL
467 of the diluted plasma stored at -20^{0}C. Plasma was further diluted 1:5 prior to ELISA with Assay
468 Buffer (PBS, 1mM Tween-20, 5% FBS). IFNγ ELISAs used the MD-1 clone for coating and a
469 biotinylated 4S.B3 clone for detection prior to visualization with a streptavidin-HRP antibody
470 (BioLegend).
471
472 *Two-photon lifetime imaging of NAD(P)H and FAD*
473 A custom-built inverted multiphoton microscope (Bruker Fluorescence Microscopy, Middleton, WI,
474 USA), was used to acquire fluorescence intensity and lifetime images. The equipment consists of
475 an ultrafast laser (Spectra Physics, Insight DSDual), an inverted microscope (Nikon, Eclipse Ti),
476 and a 40X water immersion (1.15 NA, Nikon) objective. NAD(P)H and FAD images were obtained
477 for the same field of view. FAD fluorescence was isolated using an emission bandpass filter of
478 550/100 nm and excitation wavelength of 890 nm. NAD(P)H fluorescence was isolated using an
479 emission bandpass filter of 440/80 nm and an excitation wavelength of 750 nm. Fluorescence
480 lifetime images were collected using time-correlated single-photon counting electronics (SPC-
481 150, Becker and Hickl, Brookline, MA, USA) and a GaAsP photomultiplier tube (H7422P-40,
482 Hamamatsu, Bridgewater, NJ, USA). 512x512 pixel images were obtained using a pixel dwell
483 time of 4.8 μs over 60 s total integration time. To guarantee adequate photon observations for
484 lifetime decay fits and no photobleaching, the photon count rates were maintained at 1–2 x 10^5
485 photons/s. The instrument response function was calculated from the second harmonic
486 generation of urea crystals excited at 900 nm. A Fluoresbrite YG microsphere (Polysciences Inc.,
487 Warrington, PA, USA) was imaged as a daily standard for fluorescence lifetime. The lifetime
488 decay curves for the YG microsphere standard were fit to a single exponential decay and the
489 fluorescence lifetime was measured to be 2.1 ns (n = 7), which is consistent with published values.
490 NAD(P)H and FAD intensity and lifetime images were analyzed using SPCImage software
491 (Becker &Hickl, Berlin, Germany) as described previously[58]. The fluorescence lifetime decay

492 curve was deconvolved with the instrument response function and fit to a two-component
493 exponential decay model at each pixel, $I(t) = \alpha_1 * e^{(-t/\tau_1)} + \alpha_2 * e^{(-t/\tau_2)} + C$, where I(t) represents
494 the fluorescence intensity at time t after the laser excitation pulse, α accounts for the fractional
495 contribution from each component, C represents the background light, and τ is the fluorescence
496 lifetime of each component. Since both NAD(P)H and FAD can exist in two conformational states,
497 bound, or unbound to enzymes, a two-component model was used. For NAD(P)H, the short (τ_1)
498 and long (τ_2) lifetime components correspond with the unbound and bound conformations,
499 respectively. The mean lifetime (τ_m) was calculated using $\tau_m = \alpha_1 * \tau_1 + \alpha_2 * \tau_2$, for both NAD(P)H and
500 FAD. The optical redox ratio was determined from the NAD(P)H and FAD intensity images as the
501 intensity of NAD(P)H / (NAD(P)H + FAD). Semi-automated cell segmentation was performed
502 using the cyto2 model in Cellpose, which resulted in whole-cell masks, followed by manual
503 inspection and mask corrections by a trained scientist. Using the masks, single cell features were
504 extracted including bi-exponential fit parameters (τ_1, τ_2, α_1, α_2) for NAD(P)H and FAD, NAD(P)H
505 τ_m, FAD τ_m, and the optical redox ratio. Features were calculated on a per-cell level by averaging
506 all the pixels across each cell. A minimum of 100 cells were analyzed per condition to obtain
507 statistically robust results.
508
509 *Metabolomic Assays.* ATP production rate was calculated from flow sorted CD4, CD8 and DPT
510 using an Agilent Seahorse XF Real-Time ATP Rate Assay Kit using a Seahorse XF/XFe96
511 analyzer and following the manufacturer's instructions.
512
513 *Bioluminescent Imaging.* A total of $1E^6$ luciferase positive NALM-6 cells were injected retro-
514 orbitally seven days prior to human T cell transplantation as described above. Luminescence
515 detection was gathered at the indicated times using an IVIS Spectrum In Vivo Imaging System

516 (PerkinElmer). Briefly, mice were anesthetized and intraperitoneally injected with 100μL of D-
517 luciferin at 30mg/mL with luminescence obtained approximately 15 minutes later.
518
519 *Statistics.* Graphs and statistical tests were completed using GraphPad Prism 6. All significance
520 tests were performed using either unpaired parametric (for linear data) or non-parametric (for
521 logarithmic data) t -tests.
522
523 *Study Approval.* All work involving human cells and tissues was performed in accordance with
524 IRB protocol 2014-0806 (C.M.C.). All animal work performed in accordance with UW-Madison
525 IACUC approved protocol number M005915-R01 (C.M.C.).
526
527 **Author Contributions**
528 N.J.H., J.E.G., P.H. and C.M.C. designed the study; N.J.H., D.T. and J.R. performed experiments;
529 N.J.H., J.R., S.M. and E.C.G. analyzed the data; K.N., A.W.H., N.C., M.C.S. J.E.G. and P.H.
530 provided resources; N.J.H. and C.M.C. drafted the manuscript. All authors revised and approved
531 the manuscript.
532
533 **Grant Support**
534 The authors would like to thank the University of Wisconsin Carbone Cancer Center (UWCCC)
535 Flow Cytometry Core Facility and the UWCCC Experimental Animal Pathology Laboratory, who
536 are supported by NIH/NCI P30-CA014520. The authors also utilized the University of Wisconsin-
537 Madison Biotechnology Center Bioinformatics Core Facility for the analysis of RNA-sequencing
538 data. This work was supported in part by NIH/NIAID T32-AI125231 (N.J.H), NIH/NHLBI T32-
539 HL07899 (N.J.H.), NIH/NCATS UL1-TR002373 (N.J.H), the Cormac Pediatric Leukemia
540 Fellowship (N.J.H) and the Stem Cell and Regenerative Medicine Center Fellowship (N.J.H.).
541 Additional funding includes NIH/NIAID R21-AI116007 (J.E.G.), NIH/NIAID R01-AI136500

542 (J.E.G.), St. Baldrick's-Stand Up to Cancer Pediatric Dream Team Translational Research Grant
543 SU2C-AACR-DT-27-17 (C.M.C.), American Cancer Society Research Scholar grant RSG-18-
544 104-01-LIB (C.M.C.), NIH/NCI R01-CA215461 (C.M.C.) and the MACC Fund (C.M.C). Stand Up
545 to Cancer is a division of the Entertainment Industry Foundation. Research grants are
546 administered by the American Association for Cancer Research, the scientific partner of SU2C.
547 The contents of this article do not necessarily reflect the views or policies of the Department of
548 Health and Human Services, nor does mention of trade names, commercial products, or
549 organizations imply endorsement by the US Government. None of these funding sources had any
550 input in the study design, analysis, manuscript preparation or decision to submit for publication.
551
552 The authors would like to thank the Clinical Laboratory team at UW-Health including Hugo Stoffel-
553 Rosales, Robin Rustad and Kaitlyn Walker for their help with sample collection.
554

555 **Disclosure of Conflicts of Interest**

556 C.M.C. reports honorarium from Elephas Bio, Nektar Therapeutics and Novartis, who had no input
557 in the study design, analysis, manuscript preparation or decision to submit for publication. The
558 authors declare that no other relevant financial conflicts of interest exist.
559

560 **References**

561 1. D'Souza A, Fretham C, Lee SJ, et al. Current Use of and Trends in Hematopoietic Cell Transplantation
562 in the United States. *Biol Blood Marrow Transplant*. 2020;26(8):e177–e182.
563 2. Gooptu M, Romee R, St Martin A, et al. HLA-haploidentical vs matched unrelated donor transplants
564 with posttransplant cyclophosphamide-based prophylaxis. *Blood*. 2021;138(3):273–282.
565 3. Kanate AS, Majhail NS, Savani BN, et al. Indications for Hematopoietic Cell Transplantation and
566 Immune Effector Cell Therapy: Guidelines from the American Society for Transplantation and
567 Cellular Therapy. *Biol Blood Marrow Transplant*. 2020;26(7):1247–1256.
568 4. Martinez-Cibrian N, Zeiser R, Perez-Simon JA. Graft-versus-host disease prophylaxis:
569 Pathophysiology-based review on current approaches and future directions. *Blood Reviews*.
570 2020;100792.
571 5. Ciurea SO, Zhang M-J, Bacigalupo AA, et al. Haploidentical transplant with posttransplant
572 cyclophosphamide vs matched unrelated donor transplant for acute myeloid leukemia. *Blood*.
573 2015;126(8):1033–1040.
574 6. Battipaglia G, Labopin M, Kröger N, et al. Posttransplant cyclophosphamide vs antithymocyte
575 globulin in HLA-mismatched unrelated donor transplantation. *Blood*. 2019;134(11):892–899.
576 7. Blazar BR, Hill GR, Murphy WJ. Dissecting the biology of allogeneic HSCT to enhance the GvT effect
577 whilst minimizing GvHD. *Nat Rev Clin Oncol*. 2020;
578 8. Chang Y-J, Zhao X-Y, Huang X-J. Strategies for Enhancing and Preserving Anti-leukemia Effects
579 Without Aggravating Graft-Versus-Host Disease. *Front Immunol*. 2018;9:3041.
580 9. Reddy P, Maeda Y, Liu C, et al. A crucial role for antigen-presenting cells and alloantigen expression
581 in graft-versus-leukemia responses. *Nat. Med.* 2005;11(11):1244–1249.
582 10. Meurer T, Crivello P, Metzing M, et al. Permissive HLA-DPB1 mismatches in HCT depend on
583 immunopeptidome divergence and editing by HLA-DM. *Blood*. 2021;137(7):923–928.
584 11. Mayor NP, Wang T, Lee SJ, et al. Impact of Previously Unrecognized HLA Mismatches Using
585 Ultrahigh Resolution Typing in Unrelated Donor Hematopoietic Cell Transplantation. *JCO*.
586 2021;JCO.20.03643.
587 12. Petersdorf EW, Stevenson P, Bengtsson M, et al. HLA-B leader and survivorship after HLA-
588 mismatched unrelated donor transplantation. *Blood*. 2020;136(3):362–369.
589 13. Petersdorf EW, Gooley TA, Malkki M, et al. HLA-C expression levels define permissible mismatches
590 in hematopoietic cell transplantation. *Blood*. 2014;124(26):3996–4003.
591 14. Fuchs EJ, McCurdy SR, Solomon SR, et al. HLA informs risk predictions after haploidentical stem cell
592 transplantation with posttransplantation cyclophosphamide. *Blood*. 2022;139(10):1452–1468.
593 15. Wachsmuth LP, Patterson MT, Eckhaus MA, et al. Post-transplantation cyclophosphamide prevents
594 graft-versus-host disease by inducing alloreactive T cell dysfunction and suppression. *J Clin Invest*.
595 2019;129(6):2357–2373.
596 16. Nunes NS, Kanakry CG. Mechanisms of Graft-versus-Host Disease Prevention by Post-
597 transplantation Cyclophosphamide: An Evolving Understanding. *Front Immunol*. 2019;10:2668.
598 17. Paczesny S. Biomarkers for posttransplantation outcomes. *Blood*. 2018;131(20):2193–2204.
599 18. Chen S, Zeiser R. Novel Biomarkers for Outcome After Allogeneic Hematopoietic Stem Cell
600 Transplantation. *Front Immunol*. 2020;11:1854.
601 19. Adom D, Rowan C, Adeniyan T, Yang J, Paczesny S. Biomarkers for Allogeneic HCT Outcomes. *Front*
602 *Immunol*. 2020;11:673.
603 20. Srinagesh HK, Özbek U, Kapoor U, et al. The MAGIC algorithm probability is a validated response
604 biomarker of treatment of acute graft-versus-host disease. *Blood Adv*. 2019;3(23):4034–4042.

605 21. Hotta M, Satake A, Yoshimura H, et al. Elevation of Early Plasma Biomarkers in Patients with Clinical
606 Risk Factors Predicts Increased Nonrelapse Mortality after Allogeneic Hematopoietic Stem Cell
607 Transplantation. *Transplant Cell Ther*. 2021;27(8):660.e1-660.e8.
608 22. Rowan CM, Pike F, Cooke KR, et al. Assessment of ST2 for risk of death following graft-versus-host
609 disease in pediatric and adult age groups. *Blood*. 2020;135(17):1428–1437.
610 23. Major-Monfried H, Renteria AS, Pawarode A, et al. MAGIC biomarkers predict long-term outcomes
611 for steroid-resistant acute GVHD. *Blood*. 2018;131(25):2846–2855.
612 24. Zewde MG, Morales G, Gandhi I, et al. Evaluation of Elafin as a Prognostic Biomarker in Acute Graft-
613 versus-Host Disease. *Transplantation and Cellular Therapy, Official Publication of the American*
614 *Society for Transplantation and Cellular Therapy*. 2021;27(12):988.e1-988.e7.
615 25. Subburaj D, Ng B, Kariminia A, et al. Metabolomic identification of α-ketoglutaric acid elevation in
616 pediatric chronic graft-versus-host disease. *Blood*. 2022;139(2):287–299.
617 26. Inamoto Y, Martin PJ, Lee SJ, et al. Dickkopf-related protein 3 is a novel biomarker for chronic GVHD
618 after allogeneic hematopoietic cell transplantation. *Blood Adv*. 2020;4(11):2409–2417.
619 27. McCurdy SR, Radojcic V, Tsai H-L, et al. Signatures of GVHD and Relapse after Post-Transplant
620 Cyclophosphamide Revealed by Immune Profiling and Machine Learning. *Blood*.
621 2021;blood.2021013054.
622 28. Cruz CRY, Bo N, Bakoyannis G, et al. Antigen-specific T cell responses correlate with decreased
623 occurrence of acute GVHD in a multicenter contemporary cohort. *Bone Marrow Transplant*. 2021;
624 29. Podgorny PJ, Liu Y, Dharmani-Khan P, et al. Immune cell subset counts associated with graft-versus-
625 host disease. *Biol Blood Marrow Transplant*. 2014;20(4):450–462.
626 30. Magenau JM, Qin X, Tawara I, et al. Frequency of CD4+CD25hiFOXP3+ Regulatory T Cells Has
627 Diagnostic and Prognostic Value as a Biomarker for Acute Graft-versus-Host-Disease. *Biology of*
628 *Blood and Marrow Transplantation*. 2010;16(7):907–914.
629 31. Hess NJ, Brown ME, Capitini CM. GVHD Pathogenesis, Prevention and Treatment: Lessons From
630 Humanized Mouse Transplant Models. *Frontiers in Immunology*. 2021;12:3082.
631 32. Hill GR, Betts BC, Tkachev V, Kean LS, Blazar BR. Current Concepts and Advances in Graft-Versus-
632 Host Disease Immunology. *Annu Rev Immunol*. 2021;
633 33. Teshima T, Hill GR. The Pathophysiology and Treatment of Graft-Versus-Host Disease: Lessons
634 Learnt From Animal Models. *Front Immunol*. 2021;12:715424.
635 34. Piper C, Zhou V, Komorowski R, et al. Pathogenic Bhlhe40+ GM-CSF+ CD4+ T Cells Promote Indirect
636 Alloantigen Presentation in the GI Tract during GVHD. *Blood*. 2019;
637 35. Gartlan KH, Bommiasamy H, Paz K, et al. A critical role for donor-derived IL-22 in cutaneous chronic
638 GVHD. *Am. J. Transplant.* 2018;18(4):810–820.
639 36. Piper C, Hainstock E, Yin-Yuan C, et al. Single cell immune profiling reveals a developmentally
640 distinct CD4+ GM-CSF+ T cell lineage that induces GI tract GVHD. *Blood Adv*.
641 2022;bloodadvances.2021006084.
642 37. Park S, Griesenauer B, Jiang H, et al. Granzyme A-producing T helper cells are critical for acute graft-
643 versus-host disease. *JCI Insight*. 2020;
644 38. Hashimoto K, Kouno T, Ikawa T, et al. Single-cell transcriptomics reveals expansion of cytotoxic CD4
645 T cells in supercentenarians. *Proc Natl Acad Sci U S A*. 2019;116(48):24242–24251.
646 39. Mucida D, Husain MM, Muroi S, et al. Transcriptional reprogramming of mature $CD4^+$ helper T cells
647 generates distinct MHC class II-restricted cytotoxic T lymphocytes. *Nat. Immunol.* 2013;14(3):281–
648 289.
649 40. Takeuchi A, Saito T. CD4 CTL, a Cytotoxic Subset of CD4+ T Cells, Their Differentiation and Function.
650 *Front Immunol*. 2017;8:.
651 41. Dwyer GK, Mathews LR, Villegas JA, et al. IL-33 acts as a costimulatory signal to generate
652 alloreactive Th1 cells in graft-versus-host disease. *J Clin Invest*. 2022;e150927.

42. Agle K, Vincent BG, Piper C, et al. Bim regulates the survival and suppressive capability of CD8+ FOXP3+ regulatory T cells during murine GVHD. *Blood*. 2018;132(4):435–447.
43. Beres AJ, Haribhai D, Chadwick AC, et al. CD8+ Foxp3+ regulatory T cells are induced during graft-versus-host disease and mitigate disease severity. *J. Immunol.* 2012;189(1):464–474.
44. Alhaj Hussen K, Michonneau D, Biajoux V, et al. CD4+CD8+ T-Lymphocytes in Xenogeneic and Human Graft-versus-Host Disease. *Front Immunol*. 2020;11:579776.
45. Menard LC, Fischer P, Kakrecha B, et al. Renal Cell Carcinoma (RCC) Tumors Display Large Expansion of Double Positive (DP) CD4+CD8+ T Cells With Expression of Exhaustion Markers. *Front Immunol*. 2018;9:2728.
46. Choi YJ, Park H-J, Park HJ, Jung KC, Lee J-I. CD4hiCD8low Double-Positive T Cells Are Associated with Graft Rejection in a Nonhuman Primate Model of Islet Transplantation. *J Immunol Res*. 2018;2018:3861079.
47. Zahran AM, Saad K, Elsayh KI, Alblihed MA. Characterization of circulating CD4+ CD8+ double positive and CD4- CD8- double negative T-lymphocyte in children with β-thalassemia major. *Int. J. Hematol.* 2017;105(3):265–271.
48. Quandt D, Rothe K, Scholz R, Baerwald CW, Wagner U. Peripheral CD4CD8 double positive T cells with a distinct helper cytokine profile are increased in rheumatoid arthritis. *PLoS ONE*. 2014;9(3):e93293.
49. Nascimbeni M, Pol S, Saunier B. Distinct CD4+CD8+ Double-Positive T Cells in the Blood and Liver of Patients during Chronic Hepatitis B and C. *PLOS ONE*. 2011;6(5):e20145.
50. Desfrançois J, Derré L, Corvaisier M, et al. Increased frequency of nonconventional double positive CD4CD8 αβ T cells in human breast pleural effusions. *International Journal of Cancer*. 2009;125(2):374–380.
51. Nascimbeni M, Shin E-C, Chiriboga L, Kleiner DE, Rehermann B. Peripheral CD4+CD8+ T cells are differentiated effector memory cells with antiviral functions. *Blood*. 2004;104(2):478–486.
52. Egawa T. A Fateful Decision in the Thymus Controlled by the Transcription Factor ThPOK. *J.I.* 2021;206(9):1981–1982.
53. Overgaard NH, Jung J-W, Steptoe RJ, Wells JW. CD4+/CD8+ double-positive T cells: more than just a developmental stage? *J. Leukoc. Biol.* 2015;97(1):31–38.
54. Hess NJ, Hudson AW, Hematti P, Gumperz JE. Early T Cell Activation Metrics Predict Graft-versus-Host Disease in a Humanized Mouse Model of Hematopoietic Stem Cell Transplantation. *J. Immunol.* 2020;205(1):272–281.
55. Hess NJ, S Bharadwaj N, Bobeck EA, et al. iNKT cells coordinate immune pathways to enable engraftment in nonconditioned hosts. *Life Sci Alliance*. 2021;4(7):.
56. Walsh AJ, Mueller K, Tweed K, et al. Classification of T-cell activation via autofluorescence lifetime imaging. *Nat Biomed Eng*. 2021;5(1):77–88.
57. Samimi K, Contreras Guzman E, Trier SM, et al. Time-domain single photon-excited autofluorescence lifetime for label-free detection of T cell activation. *Opt Lett*. 2021;46(9):2168–2171.
58. Sharick JT, Walsh CM, Sprackling CM, et al. Metabolic Heterogeneity in Patient Tumor-Derived Organoids by Primary Site and Drug Treatment. *Front Oncol*. 2020;10:553.

695 **Figure Legends**

696

697 **Figure 1. Post-transplant T cell metrics are predictive of allo-HSCT recipient disease**
698 **outcomes.**

699 (A) Schematic depicting the study outline. 35 allo-HSCT recipients had weekly blood samples
700 collected and processed without freezing. (B) Dot plots taken from five concatenated allo-HSCT
701 recipients who did not develop GVHD and those that developed ≥ grade 2 GVHD. Yellow box
702 indicates gating strategy for each T cell metric analyzed. (C-D) Samples collected between the
703 day 7 and 17 collection intervals were used for the analysis in (C) while samples collected
704 between the day 22 and 83 collection intervals were further normalized to each patient's date of
705 GVHD diagnosis (or day 54 for patient without GVHD) and used in (D). Each T cell metric was
706 analyzed in three binary tests shown in the bar graphs (left columns) with any tests showing
707 significance further analyzed by ROC (right columns). The mean, 95 confidence interval,
708 significance values and AUC are indicated in each graph. Each sample was treated independently
709 in these analyses. (E-F) T cell metrics exhibiting predictive value in each allo-HSCT outcome
710 were combined into a mutli-parameter ROC analysis. Analysis of the day 7-17 collection intervals
711 are in (E) and the day 22-83 collection intervals further normalized to GVHD diagnosis are shown
712 in (F).

713

714 **Figure 2. DPT develop after xenogeneic transplantation and are predictive of lethal GVHD**

715 (A) Kaplan-meier survival curve and flow plots of mice transplanted with PB-MNC and
716 representative dot plots from mouse blood at three weeks post-transplant corresponding to mice
717 that did not develop GVHD (blue) and those that developed lethal GVHD (red). (B) Representative
718 imagestream visualization of human T cells isolated from mouse blood three weeks post-
719 transplant. (C) Representative dot plots of mice transplanted with either PB-, MB-, BM- or CB-
720 MNC either at the time of euthanasia (GVHD mice, bottom) or at 12 weeks post-transplant (No

721 GVHD, top). Gating and percentage of DPTs are indicated by the red box. (D) Graphical
722 representation of the data from (C) representing >8 independent experiments. (E) Percentage of
723 DPTs in the blood of mice developing GVHD (red) or no GVHD (blue) at 1-, 3- and 6-weeks post-
724 transplant. (F-H) Data from (E) separated based on the graft source used for transplantation. (I)
725 ROC analysis of the data from (F). PB (peripheral blood), MB (G-CSF mobilized peripheral blood),
726 BM (bone marrow), CB (umbilical cord blood), MNC (mononuclear cells). Parametric t-test was
727 used to determine significance. * $p<0.05$, ** $p<0.01$, *** $p<0.001$
728
729 **Figure 3. The transcriptome of DPT is unique compared to CD4 and CD8 T cells**
730 (A) Venn diagram of the number of unique and shared differentially expressed genes among the
731 three comparisons indicated. (B) Unsupervised hierarchical clustering of the RNA-seq samples
732 using the computed Pearson correlation for each pair of samples and the Euclidean distances of
733 the correlation distances determined. (C-D) Volcano plots showing the number of differentially
734 expressed genes in the DPT:CD4 (C) and DPT:CD8 (D) comparisons using a cutoff of a ≥ 1 log
735 expression difference and a p-value of 0.01. (E) List of the 63 genes differentially expressed in
736 both the DPT:CD4 and DPT:CD8 comparisons. (F) TCR clonality analysis of the TRB gene
737 segments. Total number of unique TRB clones is indicated while the ten clones with the highest
738 frequency are colored in the pie graph.
739
740 **Figure 4. DPT Display A Transitional Expression Profile But With Reduced Expression of**
741 **Inhibitory Receptors**
742 (A) Imagestream visualization of DPTs expressing NKG2D. (B-C) Fold MFI of CD4 (green), DPTs
743 (red) and CD8 T cells (blue) expression of eight pro-inflammatory (B) and five inhibitory (C) co-
744 stimulatory receptors taken from GVHD mice at 3 weeks post-transplant. Data represents the
745 average Fold MFI of > five mice. (D-L) Analysis of nine pro-inflammatory (D-I) or inhibitory
746 receptors (J-L) on the surface of CD4, DPT or CD8 T cells from the allo-HSCT patient samples

747 collected as part of our observational study. Each dot represents the average Fold MFI of that
748 marker across all samples collected for one individual patient. Each minimum of 10 patients was
749 collected for each marker. Fold MFI = median fluorescent intensity of marker / isotype control.
750 Parametric t-test was used to determine significance. * $p<0.05$, ** $p<0.01$, *** $p<0.001$
751
752 **Figure 5. DPT differentiate from CD8 T cells after transplant and gain THPOK expression.**
753 (A) Unsupervised tSNE clustering of human T cells concatenated from five GVHD mice using a
754 9-color flow cytometry panel. (B-C) Freshly isolated CD3, CD4 and CD8 PB-Tc from a healthy
755 donor were transplanted into mice. Representative dot plots show the percentage of DPT in
756 mouse blood at three weeks post-transplant (B) with the percentage of DPT quantified in (C). (D)
757 Five mice transplanted with PB-MNC for 3 weeks were euthanized and the human cells isolated
758 from GVHD tissues prior to flow-sorting of the CD4 and CD8 T cells. (E-F) Dot plots and bar graph
759 of the percentage of DPT in the blood of mice re-transplanted with flow-sorted CD4 and CD8 T
760 cells three weeks post-transplant. Each dot represents an individual mouse. (G-J) Schematic
761 showing the standard expression dynamic of the transcription factors RUNX3 and THPOK in CD8
762 and CD4 T cells (G). (H) Table showing the fold change and p-value of RUNX3 and THPOK
763 (ZBTB7B) from our RNA-seq dataset. (I-J) Histograms and bar graphs of the Fold MFI of THPOK
764 and RUNX3 expression in CD4, DPT and CD8 T cells from GVHD mice. Fold MFI = median
765 fluorescent intensity of marker / isotype control. Parametric t-test was used to determine
766 significance. * $p<0.05$, ** $p<0.01$, *** $p<0.001$
767
768 **Figure 6. DPT cells exhibit a metabolically unique signature from other T cells.**
769 (A) Representative images from live-cell imaging of NAD(P)H τm (0.5-1.5 ns), FAD τm (0.3-1.3
770 ns), and optical redox ratio images (shown are 6 image sets of 24 sets) from flow-sorted CD4,
771 CD8 and DPT from GVHD mice. All cells were cultured for 48hrs but activated cells were also
772 stimulated with CD3/CD28/CD2 12hrs prior to imaging. Scale bar at top left, 25 μm. (B) Scatter

773 plots of the optical redox ratio (NAD(P)H / (NAD(P)H + FAD), mean NAD(P)H lifetime in ns, mean
774 FAD lifetime in ns, % unbound NAD(P)H, % protein-bound FAD. Each dot represents a single cell
775 with mean at center and error bars representing 1 standard deviation. (C-D) Confusion matrix (C)
776 and ROC curve (D) of a random forest classifier trained on the 10 OMI parameters (NAD(P)H and
777 FAD τ1, τ2, α1, α2, τm) for classification of DPT cells from CD4 and CD8 T cells. (E) UMAP
778 dimensionality reduction analysis of OMI parameter results (τ1, τ2, α1, α2, τm) for both NAD(P)H
779 and FAD. (F) Seahorse analysis of the ATP production rate of flow-sorted CD4, DPT and CD8 T
780 cells. Parametric t-test was used to determine significance. * $p<0.05$, ** $p<0.01$, *** $p<0.001$, ****
781 $p<0.0001$.Cell counts for each population: 365 CD4 ctrl, 598CD4 act, 199 DPT ctrl, 155 DPT act,
782 103 CD8 ctrl, 119 CD8 act.
783
784 **Figure 7. DPTs are sufficient to mediate GVHD pathology.**
785 (A) Schematic of experimental design. (B-G) Kaplan-meier survival curve (B) and GVHD score
786 (C) of mice transplanted with flow-sorted CD4, DPT and CD8 T cells from five pooled GVHD mice.
787 (D) Quantification of T cells numbers in GVHD target organs at time of euthanasia. Representative
788 H&E staining of liver and lung sections from transplanted mice (E) and histological scoring (F).
789 (G) Quantification of IFNγ levels in the plasma of transplanted mice. (H-I) Splenic T cells from
790 GVHD mice were cultured overnight with either Brefeldin A alone or Brefeldin A with a 4-hour
791 PMA/ionomycin stimulation prior to ICS staining of the indicated cytokine. Data is compiled from
792 4-13 mice. Non-parametric t-tests were used for determining significance between T cell numbers
793 while parametric t-tests were used for all other analyses. * $p<0.05$, ** $p<0.01$, *** $p<0.001$
794
795 **Figure 8. DPTs have limited GVL activity relative to CD4 and CD8 T cells.**
796 (A) Schematic of experiment design. The B-ALL cell line NALM-6 was transplanted for (B-G) and
797 RS4;11 for (H-K). (B-G) Kaplan-meier survival curve (B), IVIS images (C), quantification of the
798 number of NALM-6 (D) and T cells (E) in the blood and IFNγ levels in the plasma (F). (G) NALM-

799 6 cells pre-loaded with Calcein dye were co-cultured with flow-sorted CD4, DPT and CD8 T cells
800 for four hours and supernatants quantified for the presence of calcein. Data is expressed relative
801 to a max kill condition using Triton-X. (H-K) Kaplan-meier survival curve (H), quantification of
802 RS4;11 (I) and T cells in the blood (J) and IFNγ in the plasma (K) of mice transplanted with
803 RS4;11. Non-parametric t-tests were used to determine significance for the quantification of B-
804 ALL and T cell numbers while parametric t-tests were used for all other analyses. * $p<0.05$, **
805 $p<0.01$

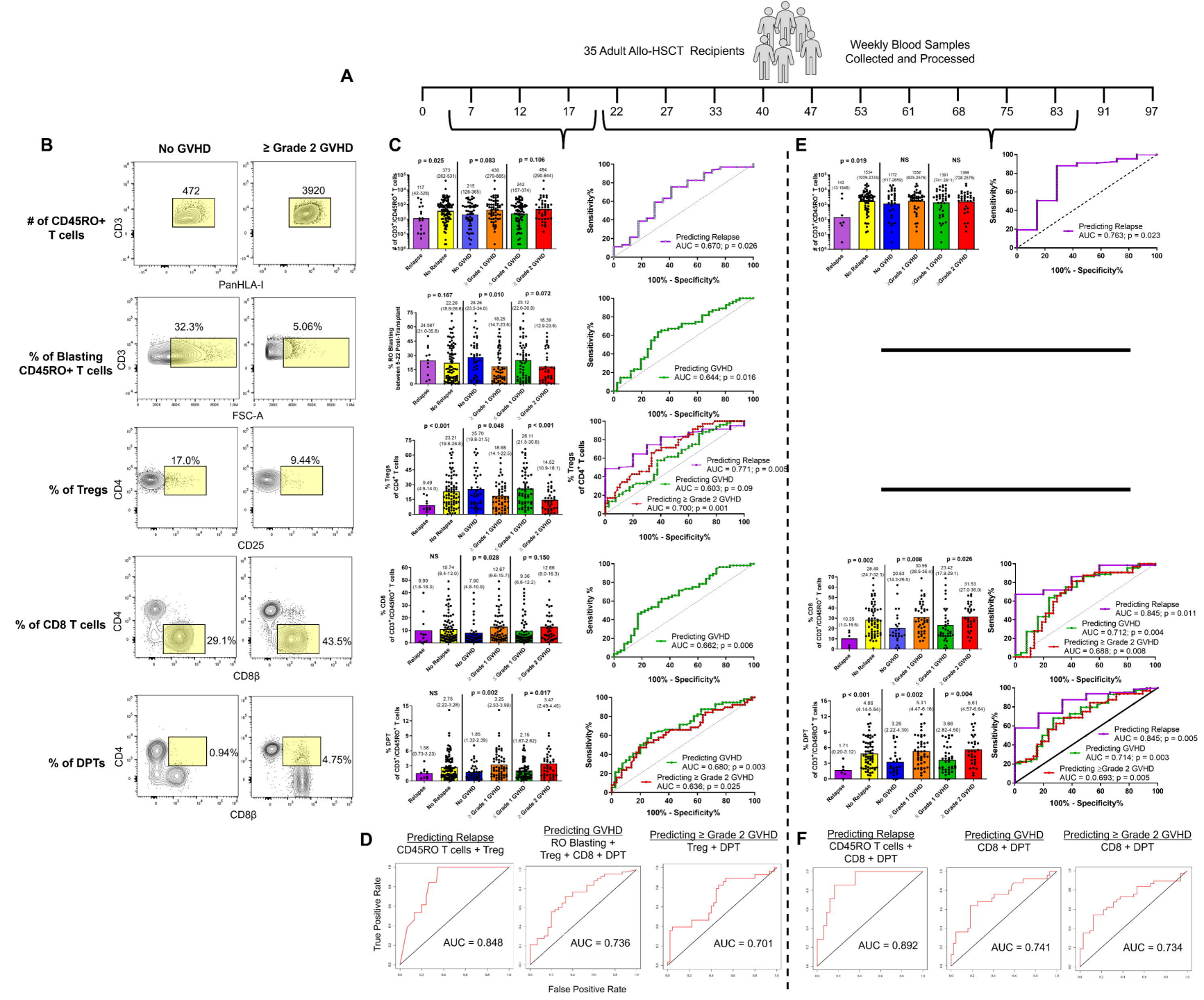
A
35 Adult Allo-HSCT Recipients
Weekly Blood Samples Collected and Processed
0 7 12 17 22 27 33 40 47 53 61 68 75 83 91 97
B
No GVHD
≥ Grade 2 GVHD
# of CD45RO+ T cells
472
3920
PanHLA-I
% of Blasting CD45RO+ T cells
32.3%
5.06%
FSC-A
% of Tregs
17.0%
9.44%
CD25
% of CD8 T cells
29.1%
43.5%
CD8β
% of DPTs
0.94%
4.75%
C
Predicting Relapse AUC = 0.670; p = 0.026
Predicting GVHD AUC = 0.644; p = 0.016
Predicting Relapse AUC = 0.771; p = 0.005
Predicting GVHD AUC = 0.603; p = 0.09
Predicting ≥ Grade 2 GVHD AUC = 0.700; p = 0.001
Predicting GVHD AUC = 0.662; p = 0.006
Predicting GVHD AUC = 0.680; p = 0.003
Predicting ≥ Grade 2 GVHD AUC = 0.636; p = 0.025
E
Predicting Relapse AUC = 0.763; p = 0.023
Predicting Relapse AUC = 0.845; p = 0.011
Predicting GVHD AUC = 0.712; p = 0.004
Predicting ≥ Grade 2 GVHD AUC = 0.688; p = 0.008
Predicting Relapse AUC = 0.845; p = 0.005
Predicting GVHD AUC = 0.714; p = 0.003
Predicting ≥Grade 2 GVHD AUC = 0.0.693; p = 0.005
D
Predicting Relapse CD45RO T cells + Treg
Predicting GVHD RO Blasting + Treg + CD8 + DPT
Predicting ≥ Grade 2 GVHD Treg + DPT
AUC = 0.848
AUC = 0.736
AUC = 0.701
True Positive Rate
False Positive Rate
F
Predicting Relapse CD45RO T cells + CD8 + DPT
Predicting GVHD CD8 + DPT
Predicting ≥ Grade 2 GVHD CD8 + DPT
AUC = 0.892
AUC = 0.741
AUC = 0.734

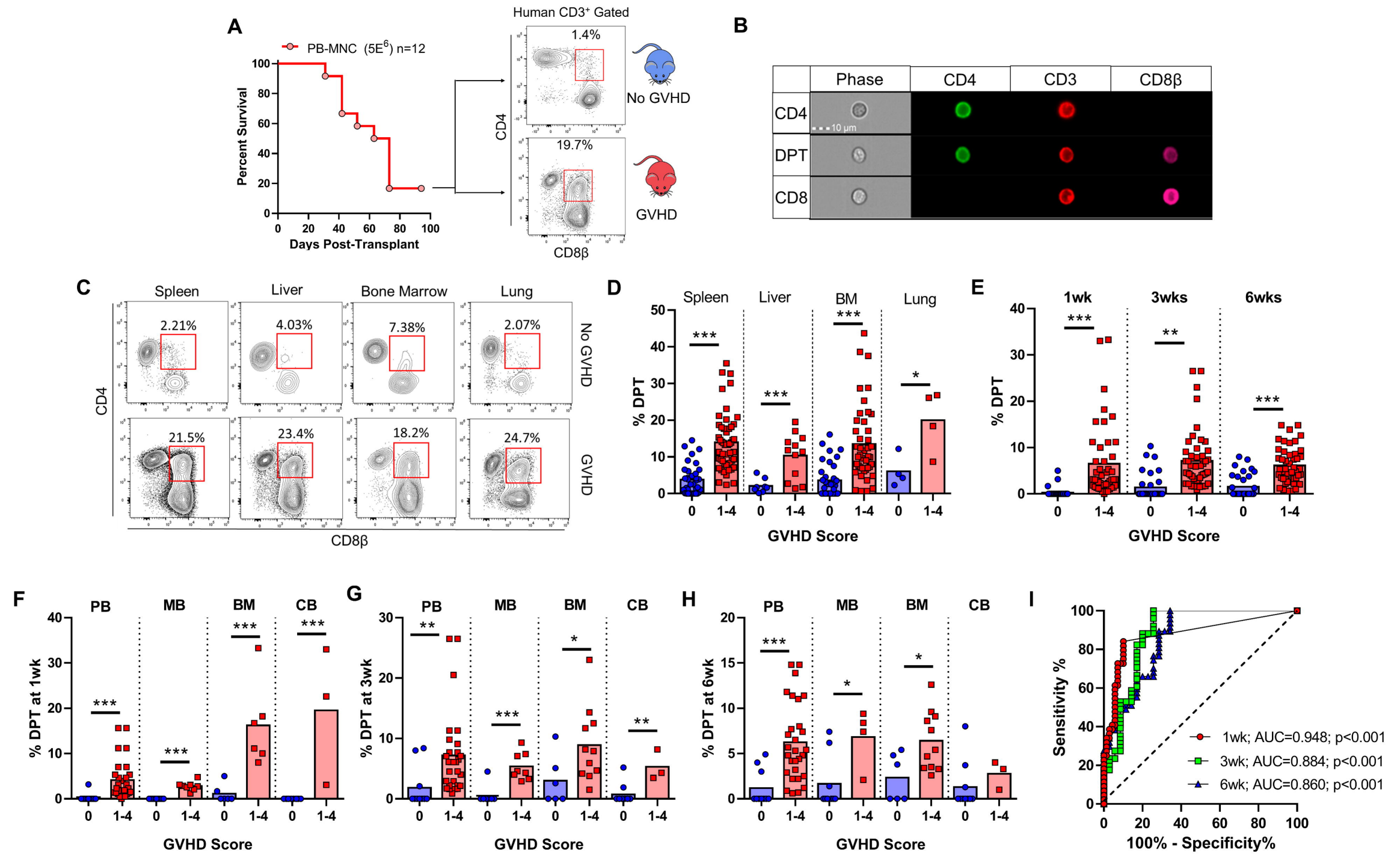
A
PB-MNC (5E6) n=12
Percent Survival
Days Post-Transplant
Human CD3+ Gated
1.4%
19.7%
CD4
CD8β
No GVHD
GVHD
B
Phase
CD4
CD3
CD8β
DPT
CD8
10 µm
C
Spleen
Liver
Bone Marrow
Lung
2.21%
4.03%
7.38%
2.07%
21.5%
23.4%
18.2%
24.7%
No GVHD
GVHD
D
% DPT
GVHD Score
E
1wk
3wks
6wks
F
PB
MB
BM
CB
% DPT at 1wk
G
% DPT at 3wk
H
% DPT at 6wk
I
Sensitivity %
100% - Specificity%
1wk; AUC=0.948; p<0.001
3wk; AUC=0.884; p<0.001
6wk; AUC=0.860; p<0.001

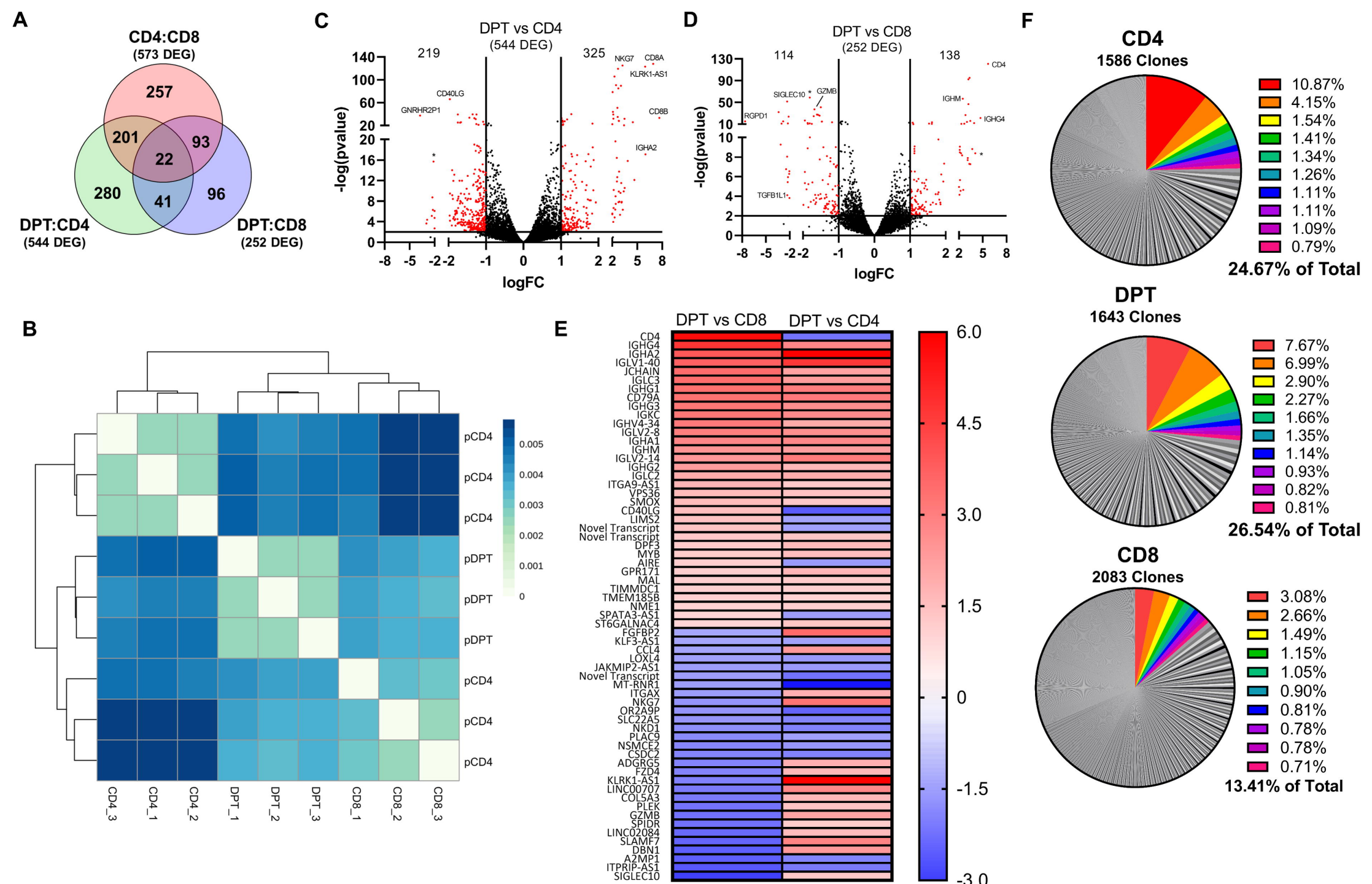
A
CD4:CD8
(573 DEG)
257
201
93
22
280
41
96
DPT:CD4
(544 DEG)
DPT:CD8
(252 DEG)
C
DPT vs CD4
(544 DEG)
219
325
NKG7
CD8A
KLRK1-AS1
CD40LG
GNRHR2P1
CD8B
IGHA2
-log(pvalue)
logFC
D
DPT vs CD8
(252 DEG)
114
138
CD4
SIGLEC10
GZMB
IGHM
IGHG4
RGPD1
TGFB1L1
-log(pvalue)
logFC
F
CD4
1586 Clones
10.87%
4.15%
1.54%
1.41%
1.34%
1.26%
1.11%
1.11%
1.09%
0.79%
24.67% of Total
DPT
1643 Clones
7.67%
6.99%
2.90%
2.27%
1.66%
1.35%
1.14%
0.93%
0.82%
0.81%
26.54% of Total
CD8
2083 Clones
3.08%
2.66%
1.49%
1.15%
1.05%
0.90%
0.81%
0.78%
0.78%
0.71%
13.41% of Total
B
pCD4
pDPT
CD4_3
CD4_1
CD4_2
DPT_1
DPT_2
DPT_3
CD8_1
CD8_2
CD8_3
E
DPT vs CD8
DPT vs CD4
CD4
IGHG4
IGHA2
IGLV1-40
JCHAIN
IGLC3
IGHG1
CD79A
IGHG3
IGKC
IGHV4-34
IGLV2-8
IGHA1
IGHM
IGLV2-14
IGHG2
IGLC2
ITGA9-AS1
VPS36
SMOX
CD40LG
LIMS2
Novel Transcript
Novel Transcript
DPF3
MYB
AIRE
GPR171
MAL
TIMMDC1
TMEM185B
NME1
SPATA3-AS1
ST6GALNAC4
FGFBP2
KLF3-AS1
CCL4
LOXL4
JAKMIP2-AS1
Novel Transcript
MT-RNR1
ITGAX
NKG7
OR2A9P
SLC22A5
NKD1
PLAC9
NSMCE2
CSDC2
ADGRG5
FZD4
KLRK1-AS1
LINC00707
COL5A3
PLEK
GZMB
SPIDR
LINC02084
SLAMF7
DBN1
A2MP1
ITPRIP-AS1
SIGLEC10
6.0
4.5
3.0
1.5
0
-1.5
-3.0

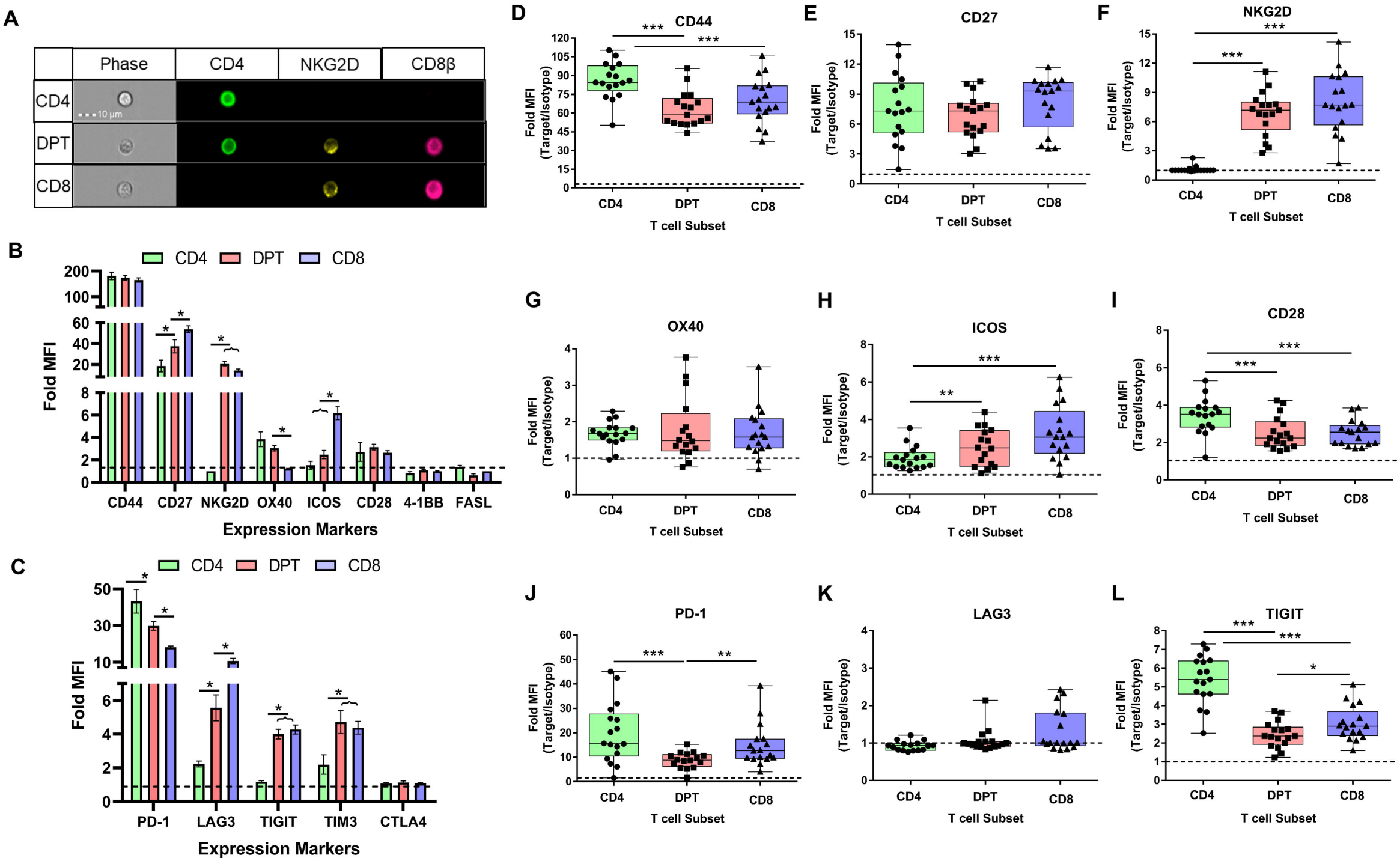
A
Phase
CD4
NKG2D
CD8β
CD4
DPT
CD8
10 µm
B
CD4
DPT
CD8
Fold MFI
CD44
CD27
NKG2D
OX40
ICOS
CD28
4-1BB
FASL
Expression Markers
C
CD4
DPT
CD8
Fold MFI
PD-1
LAG3
TIGIT
TIM3
CTLA4
Expression Markers
D
CD44
E
CD27
F
NKG2D
G
OX40
H
ICOS
I
CD28
J
PD-1
K
LAG3
L
TIGIT
Fold MFI (Target/Isotype)
T cell Subset

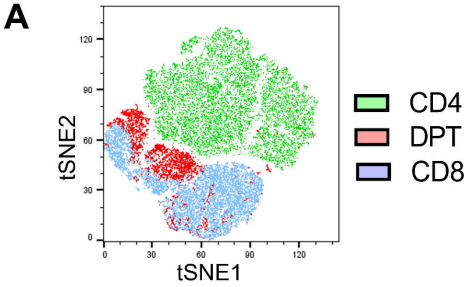

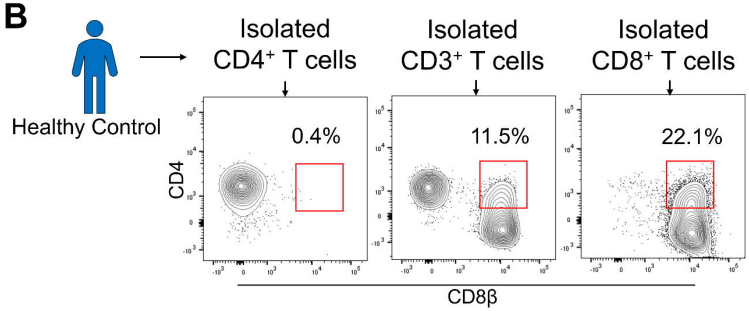

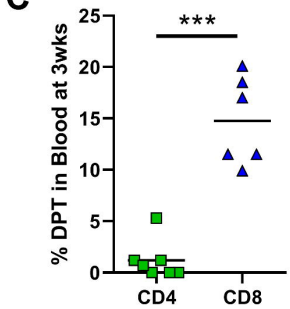

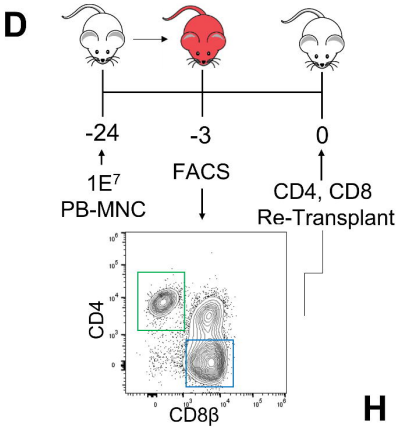

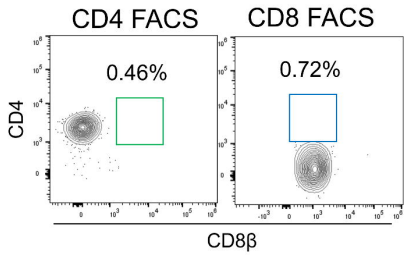

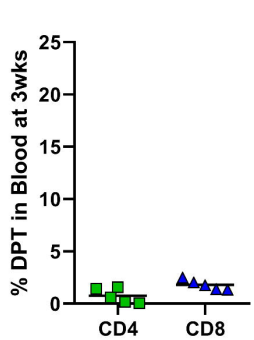

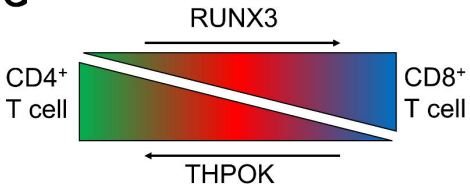

H

Comparison	Gene Name (Protein)	Fold Change	p-value
DPT:CD4	RUNX3	**0.728**	**1.15E^{-7}**
	ZBTB7B (THPOK)	-0.142	0.21
DPT:CD8	RUNX3	-.0188	0.163
	ZBTB7B (THPOK)	**1.093**	**8.14E^{11}**

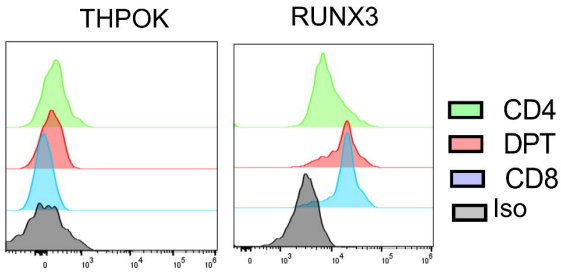

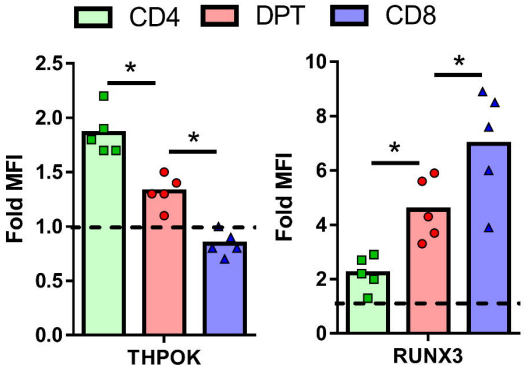

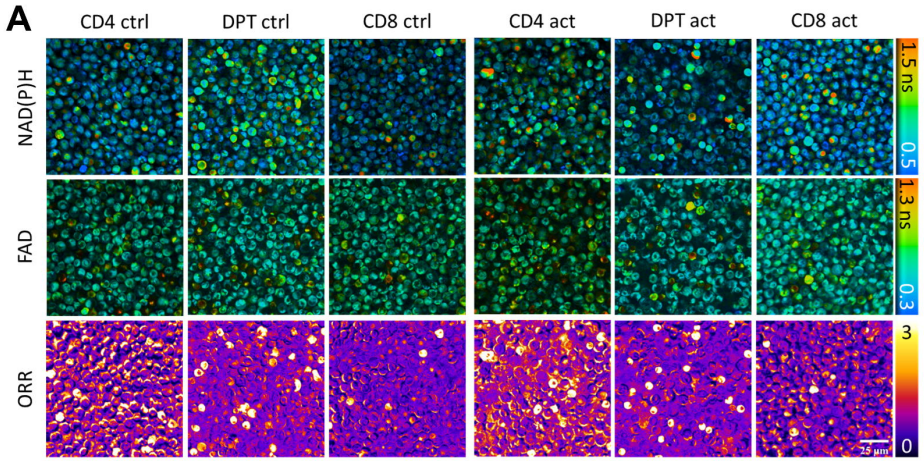

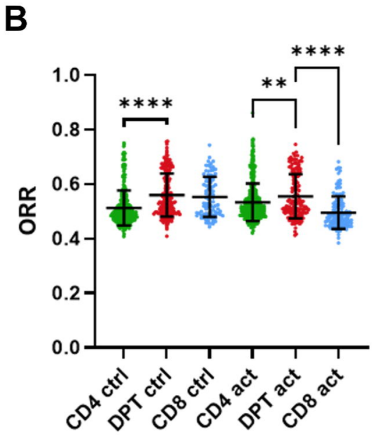

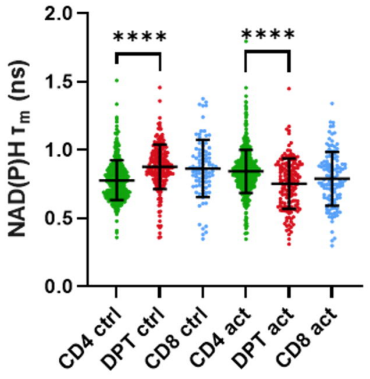

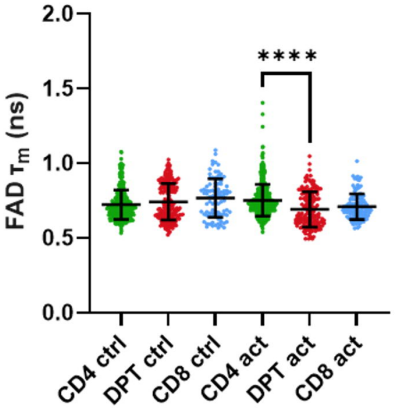

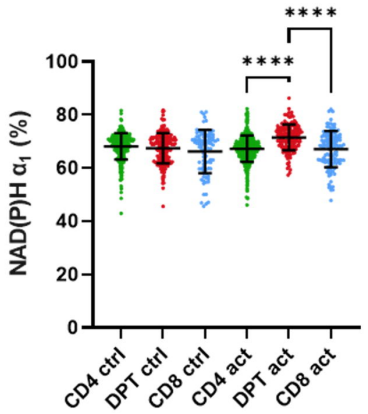

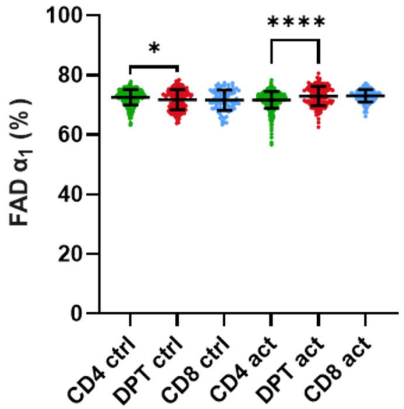

C

Random forest		Predicted Condition	
		DPT	CD4 & CD8
Actual Condition	DPT	85.64	29.17
	CD4 & CD8	14.36	70.83

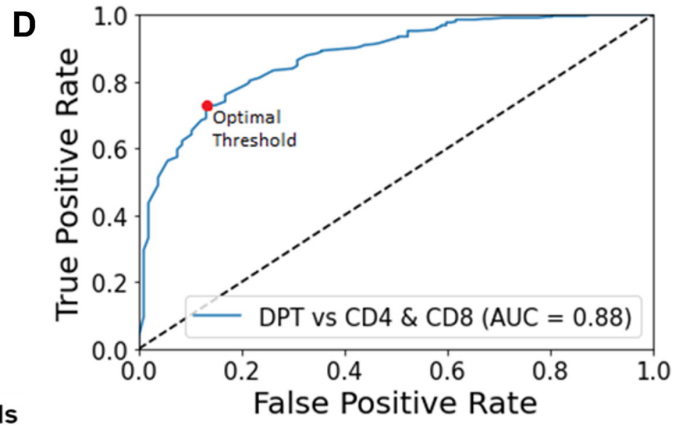

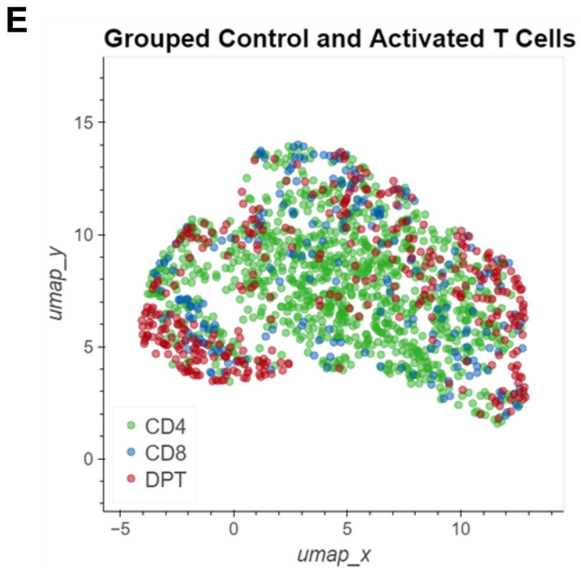

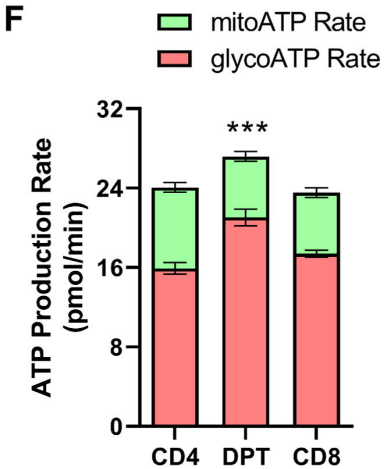

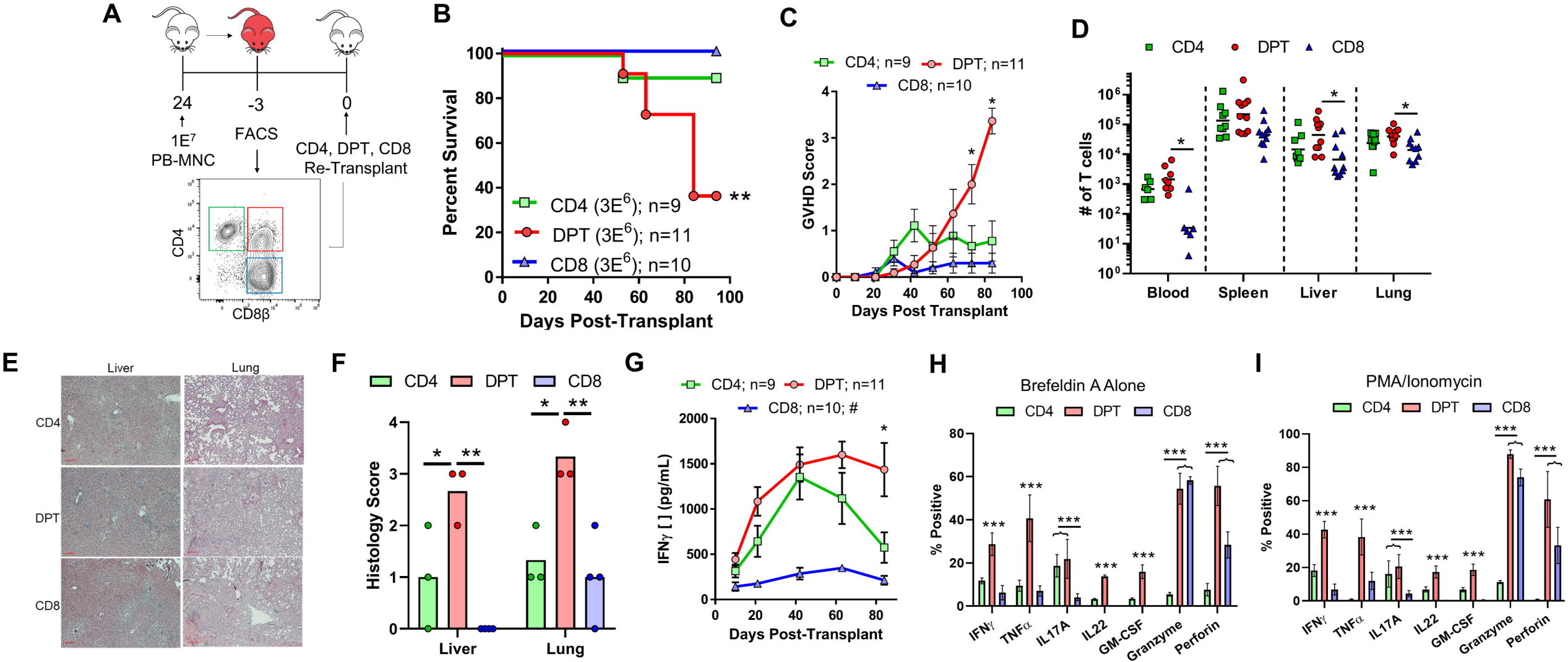
A
24
-3
0
1E7
PB-MNC
FACS
CD4, DPT, CD8
Re-Transplant
CD4
CD8β
B
Percent Survival
Days Post-Transplant
CD4 (3E6); n=9
DPT (3E6); n=11
CD8 (3E6); n=10
**
C
CD4; n=9
DPT; n=11
CD8; n=10
GVHD Score
Days Post Transplant
D
CD4
DPT
CD8
# of T cells
Blood
Spleen
Liver
Lung
E
Liver
Lung
CD4
DPT
CD8
F
CD4
DPT
CD8
Histology Score
Liver
Lung
G
CD4; n=9
DPT; n=11
CD8; n=10; #
IFNγ [ ] (pg/mL)
Days Post-Transplant
H
Brefeldin A Alone
CD4
DPT
CD8
% Positive
IFNγ
TNFα
IL17A
IL22
GM-CSF
Granzyme
Perforin
I
PMA/Ionomycin
CD4
DPT
CD8
% Positive
IFNγ
TNFα
IL17A
IL22
GM-CSF
Granzyme
Perforin

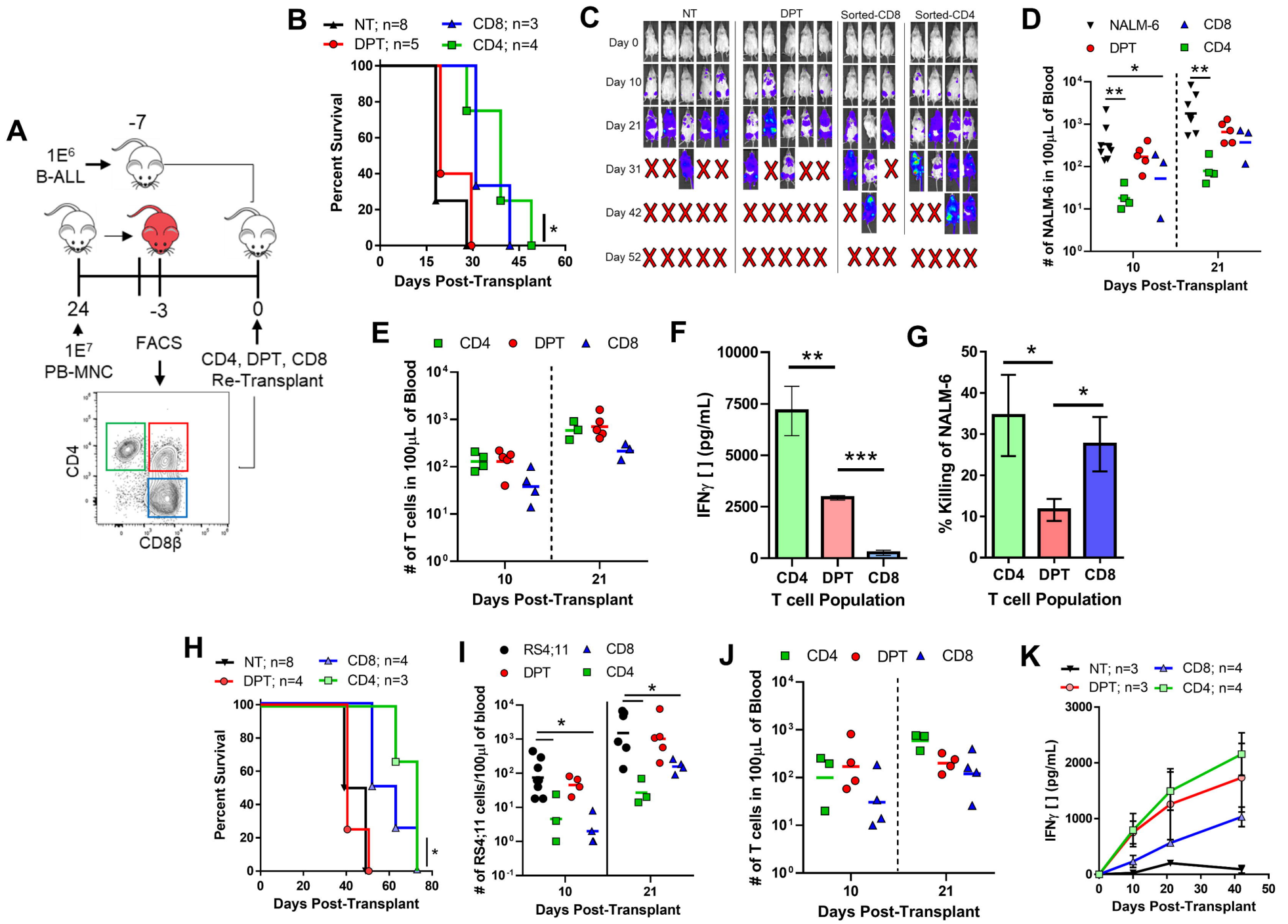
A
-7
1E6
B-ALL
24
-3
0
1E7
PB-MNC
FACS
CD4, DPT, CD8
Re-Transplant
CD4
CD8β
B
NT; n=8
DPT; n=5
CD8; n=3
CD4; n=4
Percent Survival
Days Post-Transplant
C
NT
DPT
Sorted-CD8
Sorted-CD4
Day 0
Day 10
Day 21
Day 31
Day 42
Day 52
D
NALM-6
DPT
CD8
CD4
# of NALM-6 in 100μL of Blood
Days Post-Transplant
E
CD4
DPT
CD8
# of T cells in 100μL of Blood
Days Post-Transplant
F
IFNγ [ ] (pg/mL)
CD4
DPT
CD8
T cell Population
G
% Killing of NALM-6
CD4
DPT
CD8
T cell Population
H
NT; n=8
DPT; n=4
CD8; n=4
CD4; n=3
Percent Survival
Days Post-Transplant
I
RS4;11
DPT
CD8
CD4
# of RS4;11 cells/100μl of blood
Days Post-Transplant
J
CD4
DPT
CD8
# of T cells in 100μL of Blood
Days Post-Transplant
K
NT; n=3
DPT; n=3
CD8; n=4
CD4; n=4
IFNγ [ ] (pg/mL)
Days Post-Transplant